

November 2017

Large Area Sintering Test Platform Design and Preliminary Study on Cross Sectional Resolution

Christopher J. Gardiner

University of South Florida, gardinerc@mail.usf.edu

Follow this and additional works at: <http://scholarcommons.usf.edu/etd>

 Part of the [Mechanical Engineering Commons](#)

Scholar Commons Citation

Gardiner, Christopher J., "Large Area Sintering Test Platform Design and Preliminary Study on Cross Sectional Resolution" (2017).
Graduate Theses and Dissertations.

<http://scholarcommons.usf.edu/etd/7026>

This Thesis is brought to you for free and open access by the Graduate School at Scholar Commons. It has been accepted for inclusion in Graduate Theses and Dissertations by an authorized administrator of Scholar Commons. For more information, please contact scholarcommons@usf.edu.

Large Area Sintering Test Platform Design and Preliminary Study on Cross Sectional Resolution

by

Christopher J. Gardiner

A thesis submitted in partial fulfillment
of the requirements for the degree of
Master of Science in Mechanical Engineering
Department of Mechanical Engineering
College of Engineering
University of South Florida

Major Professor: Nathan B. Crane, Ph.D.
David Murphy, Ph.D.
Tansel Yucelen, Ph.D.

Date of Approval:
October 23, 2017

Keywords: Additive Manufacturing, Powder Bed Sintering, Controls, Nylon 12, Heat Transfer

Copyright © 2017, Christopher J. Gardiner

DEDICATION

I dedicate this thesis to my parents and closest friends, who have taught me to strive for success and to never give up.

ACKNOWLEDGEMENTS

This thesis benefitted substantially from the guidance of my advisor Dr. Nathan Crane who always provided exceptional direction and scientific insight. USF Doctoral candidate Justin Nussbaum also made substantial contributions to this work with his previous creation and study of a first generation system, and intellectual and physical contributions to the system built and tested in this thesis. USF undergraduates Megan Hostetter and Carlos Peña are recognized for their physical contributions to the hardware and documentation of the system, while undergraduate Coralie Madera-Caban is recognized for her contribution in assisting in the software development for the system.

TABLE OF CONTENTS

LIST OF TABLES	iv
LIST OF FIGURES	v
ABSTRACT	vii
CHAPTER 1: INTRODUCTION	1
1.1 Background on Additive Manufacturing.....	1
1.2 Selective Laser Sintering.....	1
1.3 Large Area Sintering	2
1.3.1 Large Area Sintering Overview	2
1.3.2 Motivation for Investigation of LAS.....	2
1.4 Thesis Statement	4
1.5 Chapter Overview	4
CHAPTER 2: MECHANISMS OF LARGE AREA SINTERING	6
2.1 Heat Transfer in LAS	6
2.1.1 Heat Sources.....	7
2.1.1.1 Sintering Radiation Source	7
2.1.2 Energy Density.....	8
2.1.2.1 Necessary Additional Heating Resources	9
2.1.3 Heating a Square of Powder.....	10
2.1.4 Melting and Crystallization.....	12
2.1.5 Melt Pool Propagation	13
CHAPTER 3: SYSTEM HARDWARE DESIGN	15
3.1 System Overview	15
3.2 Build Chamber / System Chassis	16
3.3 Powder Bed	18
3.3.1 Components / Construction.....	18
3.3.2 Mechanical Control.....	20
3.3.3 Thermal Control.....	21
3.3.3.1 Powder Bed Bulk Heating.....	21
3.3.3.2 Powder Surface Heating.....	22
3.4 Layer Deposition.....	22
3.4.1 Powder Deposition.....	22
3.4.2 Powder Layer Spreading.....	23
3.5 Projector	25
3.5.1 Models Used	25

3.5.2	Modifications Made	25
3.6	Thermal Camera	27
3.7	Control Hardware	29
3.7.1	Temperature Control	31
3.7.2	Projector Control	31
CHAPTER 4: SYSTEM CONTROL		32
4.1	Motivation for Closed Loop Control	32
4.2	Characterization of Projected Radiation	33
4.3	Geometric Calibration	34
4.3.1	Warping the Thermal Image	35
4.3.2	Cropping the Warped Thermal Image	37
4.3.3	Configuration File	37
4.3.4	Calibration Accuracy	38
4.4	Control Architecture	40
4.4.1	Choosing a Processing Resolution	40
4.4.2	Generating the Control Signal	41
4.4.3	Normalizing the Reference Image	41
4.4.4	Error Matrix	41
4.4.5	Control Algorithm	42
4.4.5.1	Proportional Control	43
4.4.5.2	Additional Control Signal Conditioning	43
4.4.6	Generating the Control Signal Image	44
4.4.7	Sending the Control Signal Image to the Projector	44
4.5	Gray Scale Calibration	44
CHAPTER 5: SYSTEM COMMISSIONING		46
5.1	Sintering Substrate	46
5.2	Powder Bed Conduction Heating	47
5.3	Preliminary Sintering Trials	48
5.3.1	Depositing Layers	48
5.3.2	Zeroing the Z-axis	49
5.3.3	Sintering Base Layers	49
5.3.4	Closed Loop Preheat	50
5.3.5	Sintering	51
5.3.6	Sintering Uniformity	51
5.4	LAS Performance Stability	52
5.4.1	Projector Power Uniformity	53
5.5	Trial Procedure	54
CHAPTER 6: EXPERIMENTATION		56
6.1	Experimental Goals	56
6.2	Cross Section Tested	57
6.2.1	Making the Cross Section Reference Images	57
6.2.2	High Aspect Ratio Notches	57
6.3	Experimental Trials	58
6.3.1	Independent Variables Tested	58

6.3.2	List of Experiments.....	58
6.4	Results.....	58
6.4.1	Thermal Data	58
6.4.1.1	Thermal Cross Sections	59
6.4.1.2	Thermal Data Graphs	59
6.4.2	Geometrical Data	61
6.4.2.1	Measurement Procedure.....	61
6.4.2.2	Images	63
6.4.2.3	Graphs	64
6.4.2.4	Statistics on Significant Findings.....	66
6.5	Discussion	67
6.5.1	Notch Depths	67
6.5.2	Notch Widths	68
6.5.3	Notch Draft Angle.....	68
6.5.4	Notch Exterior Corner Radii.....	69
6.5.5	General Discussion	69
CHAPTER 7: CONCLUSION.....		70
7.1	Evaluation of Thesis Statement.....	70
7.2	Comments and Future Work Recommendations	71
7.2.1	Future Experiments	71
7.2.2	Future System Improvements	72
REFERENCES		73
APPENDIX A: PURCHASING LOCATION OF IMPORTANT COMPONENTS		75
APPENDIX B: CRITICAL MATLAB SCRIPTS		76

LIST OF TABLES

Table 3-1 Optoma X316 projector specifications	25
Table 4-1 Thermal camera calibration	36
Table 5-1 Summary of base layer power exposure intensities and times	50
Table 6-1 Summary of experimental trial parameters.	58
Table 6-2 Summary of notable statistics.....	66

LIST OF FIGURES

Figure 2.1 - Sintering melt pool penetration	7
Figure 2.2 - Light penetration as a function of layer thickness with Nylon 12 powder	8
Figure 2.3 - Heating components of powder bed.....	10
Figure 2.4 - Heating a square of powder.....	11
Figure 2.5 - Slice of temperature data for heating a square of powder.....	12
Figure 2.6 - DSC data for the Nylon 12 powder used	13
Figure 3.1 - A schematic of the full system.	16
Figure 3.2 - An isometric view of the full system.	17
Figure 3.3 - Projector mounting on a pivoting bracket.....	18
Figure 3.4 - End on view of the powder bed (movement into and out of the page)..	19
Figure 3.5 - The build plate adjustment assembly	20
Figure 3.6 - The methods of powder bed heating	21
Figure 3.7 - The layer deposition system provided consistent layers.....	23
Figure 3.8 - The powder overflow gutters	24
Figure 3.9 - The projector modifications	26
Figure 3.10 - The infrared camera orientation	28
Figure 3.11 - A schematic of the physical control of the system.....	30
Figure 3.12 - The feedback control layout.....	31
Figure 4.1 - The temperature distribution across a 12 mm circular sintering cross section	33
Figure 4.2 - Cross section reference image (left) with resulting sintered part (right)	34
Figure 4.3 - The geometric calibration	35

Figure 4.4 - An example configuration file	38
Figure 4.5 - The resolution of the thermal camera.....	39
Figure 4.6 - Feedback control loop.....	42
Figure 4.7 - Power calibration with gray scale (% brightness).....	45
Figure 5.1 - A sintered interior square	48
Figure 5.2 - G-code to deposit 50 micron layer	49
Figure 5.3 - The power uniformity of projector.....	53
Figure 6.1 - HAR interior notch reference images (left - 40 x 60; right 40 x 160 pixels).....	57
Figure 6.2 - HAR notch thermal images at 3.5 seconds into sintering	59
Figure 6.3 - Temperature response at the middle and corner of the sintering cross section.....	60
Figure 6.4 - Temperature data along a line through the cross section	60
Figure 6.5 - Visual representation of where the data was taken for figures 6.3-4.....	61
Figure 6.6 - Optical measurement of notch geometry.	62
Figure 6.7 - High aspect ratio notch specimen images	63
Figure 6.8 - Notch depth vs Aspect ratio.	64
Figure 6.9 - Draft angle vs. Aspect ratio.....	64
Figure 6.10 - Notch width (top) vs Aspect ratio.	65
Figure 6.11 - Notch width (bottom) vs. Aspect ratio.....	65
Figure 6.12 - Exterior corner radius vs Aspect ratio.....	66

ABSTRACT

Additive manufacturing involves the layer-wise patterned addition of material to create 3D parts, allowing for parts with complex geometries that traditional subtractive manufacturing processes cannot create, while offering good value for low run production parts by eliminating the cost of tooling. Large Area Sintering is a form of powder based additive manufacturing where entire layer cross sections are heated and fused in a single continuous exposure process. This layer by layer powder sintering process is similar to selective laser sintering, but by heating the cross section at a slower and controllable rate there is an opportunity to achieve tighter control over thermal history. This thesis discusses the design, construction, and validation of a large area sintering test platform, as well as a preliminary study on feature resolution. A key component of this system was the integration of an infrared camera, allowing point-wise temperature control of the sintering cross section. There is a hypothesis that longer and controlled heating rates in Large Area Sintering (in comparison to Selective Laser Sintering) would allow the capability to process a wider range of materials, and give more control over the resulting final part properties. The test platform created a repeatable test environment, and successfully demonstrated the capability for point wise temperature control of the sintering cross section, enabling the ability to examine the effects of slower controlled heating rates. Available power on the system was 2.22 W/cm^2 for heating, with a temperature control loop time of 160 – 180 ms. The results of the preliminary study on feature resolution also suggested a positive correlation between point wise closed loop temperature control and improved feature resolution, giving motivation for further study.

CHAPTER 1: INTRODUCTION

1.1 Background on Additive Manufacturing

Additive manufacturing offers a novel alternative to traditional manufacturing methods in its suitability for low volume production of components as well as its ability to create complex parts that are either difficult or impossible to create otherwise [1]. As technologies are introduced and improving, there has been a shift from using additive manufacturing solely for rapid prototyping to mainstream production applications [2]. To build consumer grade parts, the processes involved have to be able to meet the designer's needs (including the ability to use appropriate materials), as well as being economical. One technology that has strong potential in mainstream production is selective laser sintering, a process that can produce dense parts with near injection-molded component mechanical properties.

Large area sintering applies the same principles as selective laser sintering but on a much slower time scale over a much larger area (hence the name), at lower maximum temperatures. Due to these material processing differences it has potential to meet the requirements of mainstream production in ways that SLS cannot; specifically the potential to process different materials and better control some property aspects of the finished parts.

1.2 Selective Laser Sintering

In selective laser sintering, a laser is used to create a small melt pool in a thin layer of powder [3]. Using a galvanometer to direct the laser, it is scanned across the powder bed rapidly in a raster pattern to create 2D cross sections, the same way one colors in a coloring book with a marker. This high intensity heating of a small area both heats the powder particles beyond their

melting point and can leave a distorted thermal profile across the 2D cross section as the laser moves around the cross section; both of these factors can negatively affect mechanical properties of the part. With the goal of increased manufacturing throughput by increasing scan speed, the necessary accompanying laser power increase is limited by the resulting steep temperature gradients, where the powder is heated to temperatures beyond degradation temperature of the powder [4].

1.3 Large Area Sintering

1.3.1 Large Area Sintering Overview

In large area sintering (LAS), a high resolution DLP (digital light processing) projector emitting a focused white light image on a powder bed is used to heat up and fuse layers of powder particles within a 2D cross section to the previous layers in one continuous process. By sintering multiple powder layers sequentially and stacking these thin 2D cross sections, 3D parts can be created.

In practice, this patterned radiation heats the interior areas of the cross section first, because there is less unheated powder around to lose heat to. This forms a melt pool which then propagates to occupy the full shape of the sintering cross section. By taking advantage of the digital aspect of the projector, any radiation pattern can be projected onto the powder bed within resolution limits.

1.3.2 Motivation for Investigation of LAS

In all powder based sintering technologies, the fundamental requirement to sinter a layer is to heat and melt the powder through the thickness of the layer, fusing it to the layer below. In SLS a typical set of parameters for polymer sintering could be a 240 μm laser spot size scanning at 1 m/s [5], giving an exposure time of 0.24 ms. For the laser to supply sufficient energy to melt the powder in such a short time, a very steep thermal gradient must be created in the powder, with the

temperature at the top of the layer much higher than the melting temperature of the powder. This not only occurs with the goal of fusing powder in the Z-direction. In scanning adjacent lines, if the laser scans them with too short of a period in between the powder will overheat and thermally degrade. Conversely with too long of a delay ideal adhesion is not achieved [3].

In LAS, the heating rates are 4 orders of magnitude lower (on the order of seconds), requiring a much smaller thermal gradient to transfer adequate heat to fuse the layer to the layer below. Beyond this, with the addition of closed loop control it is possible to control the heating of layers and minimize overshoot past the melting point of the powder. For common materials used in SLS such as Nylon 12, this can mean less material degradation which could lead to improved mechanical properties. There is also opportunity to sinter other materials with narrow processing temperature windows and low degradation temperatures, not currently used with SLS but with a demand in industry. A good example of these would be 3d printed biomaterials to create implants for medical use, for example a bone implant material that cannot exceed 65 °C which can be fused with PCL, a biodegradable polyester with a melting temperature of 61 °C [6]. An additional benefit of the point wise temperature control is the slower and uniform cooling profile, leaving lower residual stresses in the finished part.

Beyond the ability to control the heating of sintering layers, LAS offers intriguing opportunities in manufacturing throughput. In SLS, because the laser has to raster the entire cross section of a layer, sintering time increases as the area of the area of the sintered part increases. In LAS the sintering time is much less dependent on area, with larger areas actually sintering slightly faster due to a relatively lesser amount of unheated powder around them to lose heat to. This means that in LAS as the powder bed / projected image size scales up, the volume throughput scales linearly with the area increase.

1.4 Thesis Statement

The focus of this study was the design, construction, and validation of a large area sintering test platform. The purpose of the test platform was to test the hypothesis that longer and controlled heating rates in Large Area Sintering (in comparison to Selective Laser Sintering) would allow the capability to process a wider range of materials, as well as allow more control over the resulting final part properties. In order to control these heating rates, a repeatable sintering environment was created within the test platform, and a geometrically calibrated infrared camera enabling point wise closed loop temperature control was integrated into the system. Of particular interest was the ability to test if point wise closed loop temperature control could improve feature resolution, on top of the more obvious abilities to hold the sintering cross section within a desired processing temperature window. Sample results are reported from parts printed on the system in preliminary experiments under different control conditions to validate the system performance.

1.5 Chapter Overview

With the goal to create a test platform for large area sintering, a logical start is in an investigation of the physical processes involved in LAS; this is covered in “Chapter 2: Mechanisms of Large Area Sintering”. A major focus is on the thermal gradients involved and the heating rates of cross sections as a function of local position.

“Chapter 3: System Hardware Design” explores the requirements of the test platform and how these were met from a hardware standpoint. This includes specifics on the manufactured / purchased components, and how they were used together to satisfy the requirements.

“Chapter 4: System Control” goes into thorough detail on the integration of the thermal camera. A significant part of this was the geometric calibration step to transform the skewed

thermal image into usable sintering cross section temperature data. The chapter then discusses how this data is processed in order to generate a control signal image to send to the projector.

In order to create repeatable test conditions for sintering experiments, independent variables such as preheat settings, additional radiation heating settings, base layer parameters and more had to be held constant. “Chapter 5: System Commissioning” provides an overview of the experiments conducted to understand these variables and converge to effective values for them. It also serves as a record of the validation of the system, documenting the first successfully sintered parts. Through this preliminary experimentation, a standard operating procedure was developed for sintering parts.

“Chapter 6: Experimentation” further explores the validation of the system, with a selection of parts sintered under controlled conditions. Point wise temperature control was tested and compared to open loop control for its ability to keep the sintering area within a specified temperature window, and the parts were examined in search of the impact this could have on feature resolution.

“Chapter 7: Conclusion” reflects on the overall capabilities of the system as a test platform for large area sintering. This includes changes that should be made to the system in order to increase its effectiveness. In addition to this, there is a discussion of future experiments that are anticipated to be conducted on the system.

CHAPTER 2: MECHANISMS OF LARGE AREA SINTERING

This chapter takes a closer look at the processes involved when patterned radiation is projected onto a powder layer in large area sintering, melting and fusing the layer to the previous layer. This encompasses the transfer of heat to the sintering section, thermal gradients that form as this heat propagates outwards, and propagation of the melt pool / the associated effects this has on the heat transfer to the surroundings.

2.1 Heat Transfer in LAS

The fundamental requirement for a successful sintered layer in all sintering technologies is for the fresh layer of powder to be melted through the depth of the layer and fused to the layer below. In LAS for a given layer, radiation heat flux is applied to the desired cross section, raising the temperature of the powder above the melting point to create a melt pool in the shape of the desired cross section. This melt pool must propagate in the Z-direction through the layer in all areas of the cross section, in this time the melt pool also will propagate to some degree in the X-Y plane (sintering plane, parallel to the layer plane), which can negatively impact feature resolution.

USF Doctoral candidate Justin Nussbaum implemented an elementary first generation large area sintering system. This system utilized a heated build plate on a CNC mill with provisions for manual layer spreading [7]. This system, using a nearly equivalent power projector to the equipment used in this thesis, provided some preliminary data on sintering time vs melt pool penetration depth with black Nylon 12 powder.

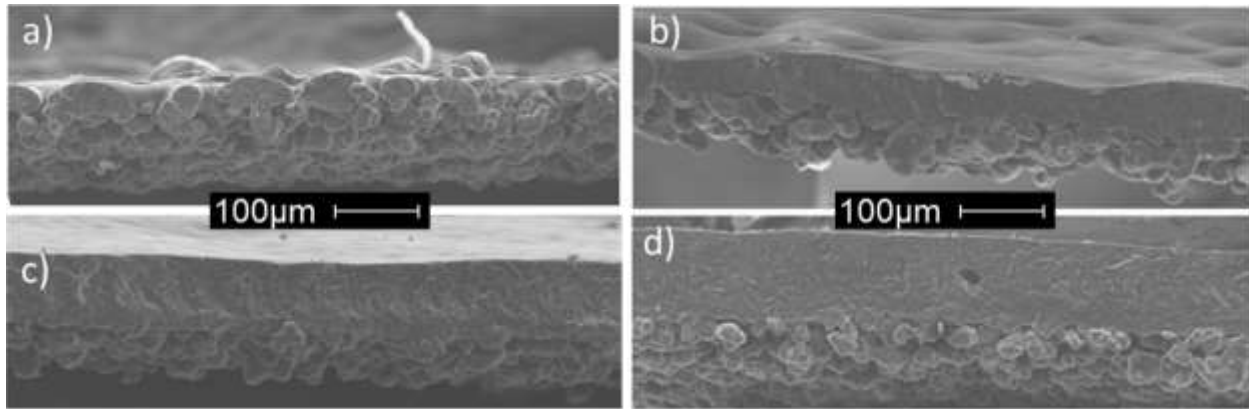


Figure 2.1 – Sintering melt pool penetration. These are single layer cross sections at various exposure times under full power on a similar system [100x magnification]; a) 1.5 s, b) 1.75 s, c) 2 s, d) 3 s. It is readily seen that in a) and b) the powder particles are not fused together in the X-Y plane, and the melt pool only successfully propagated in c) and d), with d) being the only case where the melt pool reached a depth of 100 μm , the most common polymer powder sintering layer thickness. The fundamental requirement of a successful sintered layer is that it is melted through the depth of the layer and fused to the next layer. [7]

With the fundamental idea of propagating the melt pool through the thickness of the layer with patterned radiation energy, this radiation heat transfer into the powder is counteracted by heat transfer away from the desired cross section. The cooling is characterized by heat lost within the X – Y layer plane to unheated powder around the cross section, heat conducted downward into the rest of the sintered part, and radiation / convection cooling to the surroundings. These cooling effects can cause the final melt pool geometry to stop short of the full desired cross section in the X-Y plane. Conversely, as the sintering time is increased to expand the melt pool fully, it may overrun in areas with less cooling effects (large sintering areas with minimal unheated powder around them).

2.1.1 Heat Sources

2.1.1.1 Sintering Radiation Source

The primary source of heat to sinter the desired cross section is the patterned radiation from the projector. DLP projectors are optimized to eliminate IR light to reduce heating of the digital micromirror device (DMD chip), so the light is almost entirely in the visible spectrum. In

this study nylon 12 powder was used, with the color black to absorb the largest amount of radiation energy (emissivity 0.95). The use of a projector for heating thin layers (100 μm) of this powder is validated by data characterizing the light penetration at various depths, shown in Figure 2.2. With the knowledge that light is either absorbed, transmitted, or reflected, these data showed that over 60% of the light was absorbed by what would be the first layer of powder (100 μm) and nearly 100% by 200 μm depth. This small amount of additional heat transmitted through the first layer could aid in the fusion of the two layers together, improving properties [7].

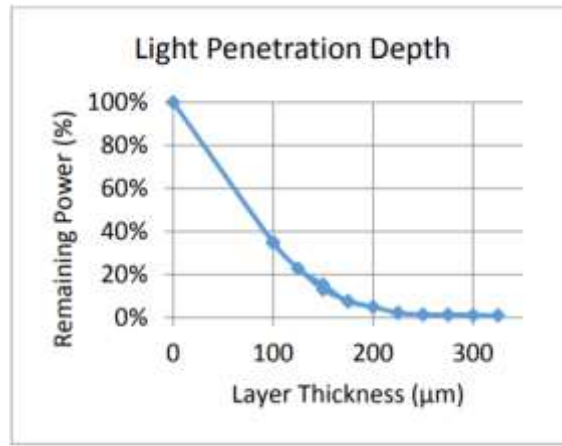


Figure 2.2 - Light penetration as a function of layer thickness with Nylon 12 powder. Powder was spread using a blade scraper system. [7]

2.1.2 Energy Density

Energy density is a measure of the amount of energy per unit volume transferred into the process material in the sintering cross section. In selective laser sintering this is calculated by the following formula [8]:

$$E_D = \frac{P}{SS \cdot H \cdot t} \quad (1)$$

where E_D = Energy Density [J/mm^3] ; P = Laser Power [W] ; SS = Scan Speed [mm/s]

H = Hatch Distance [mm] (distance between sintering lines) ; t = Layer Thickness [mm]

This can be adapted to large area sintering with the following equation for energy per unit volume, solving for radiation heat flux first:

$$q_r'' = \frac{P}{A_{max}} \quad (2)$$

$$E_D = \frac{q_r'' * t_s}{t} \quad (3)$$

where E_D = Energy Density [J/mm³]; q_r'' = radiation heat flux [W/mm²]; P = projector power (W)

A_{max} = total area of image[mm²] (not just the sintered area); t_s = sintering time (s)

t = layer thickness (mm)

For this system, with $P = 7.7$ watts and $A_{max} = 16.1$ mm x 21.5 mm the available radiation heat flux was $q_r'' = 2.22$ W/cm², which for a 4 second exposure and 100 μm layer (parameters used later in experiments) gives $E_D = 0.890$ J/mm³. In SLS it has been found that energy densities from 0.1 – 0.3 J/mm³ are most effective with Nylon 12 [3], with better properties occurring at the high end of this spectrum. An observation is that in LAS, due to the much longer exposure time a significant amount of energy can be lost to the surroundings / previously sintered layers and not put into processing the sintering cross section. This is beyond the scope of this thesis but the test platform developed will allow the quantification of this phenomenon.

2.1.2.1 Necessary Additional Heating Resources

The heat sources used in the sintering test platform are outlined in Figure 2.3. An additional external radiation source (a 60 watt 10° halogen light with mechanical dimmer switch) was used to heat the surface of the powder to reduce the energy required to sinter a cross section, as well as reduce temperature gradients in the XY plane while sintering. A third heat source is heat coming from the walls and build plate in the powder bed. This helps to control the bulk temperature of the

part / surrounding powder during subsequent layers (helps control cooling rates and recrystallization). By elevating the powder bed temperature part distortion is minimized for polymers where the crystallization temperature is well below the melting point [9]. As the layers progress and the powder bed gets deeper the heated build plate plays less of a role in heating the surface layer and the external radiation becomes a larger factor in heating the surface of the powder bed to the desired temperature (160 -165 °C).

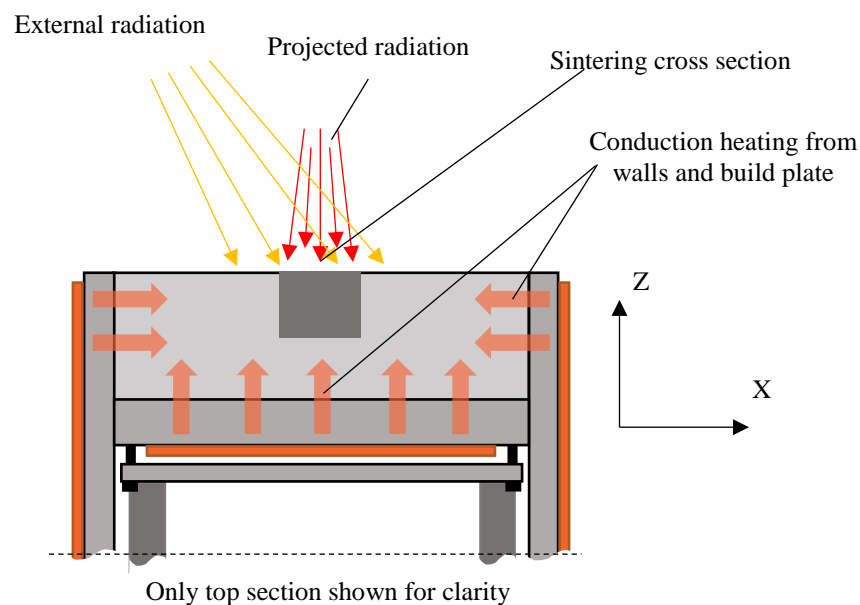


Figure 2.3 - Heating components of powder bed.

2.1.3 Heating a Square of Powder

For a given square of “on” pixels a square of powder is correspondingly heated via radiation. This differential powder element is losing heat to its surroundings along the edges where the adjacent unheated powder acts as a heat sink, while the powder particles in the center of the cross section are surrounded by other powder particles also being heated. The heat lost to surroundings via conduction is relatively proportional to the perimeter of the square being heated (distance of interface between heated powder and surrounding cool powder), while the area being

heated and thus the amount of heat going into the part for a given radiation flux is proportional to the length dimension squared. As the size of the projected profile increases, the rate at which heat can leave the cross section decreases relative to the radiation energy entering the cross section. This naturally leads to a minimum size feature that can be successfully melted into the powder for a given radiation heat flux, all other variables constant (including time and preheat).

As time progresses, temperature gradients extend outwards from the cross section and maximum cooling occurs at the corners of the heated square, which have the largest amount of unheated powder around them. This is demonstrated in Figure 2.4. Figure 2.5 shows quantitatively the temperature gradient of a slice of the heated square, they are steepest at the very edges of the patterned radiation.

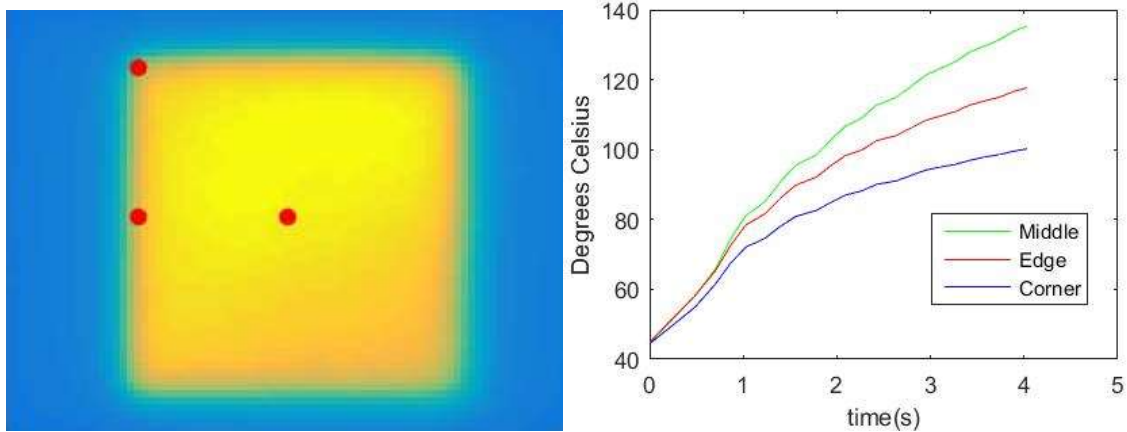


Figure 2.4 - Heating a square of powder. a) The infrared image of a square of powder with a 100% radiation power step input, with the temperature measurement points indicated b) This graph represents the temperature response in different areas of the square. The temperatures shown are at the middle, middle edge, and corner of the square. It is clear that the corner is the slowest to heat, because it is losing heat the fastest.

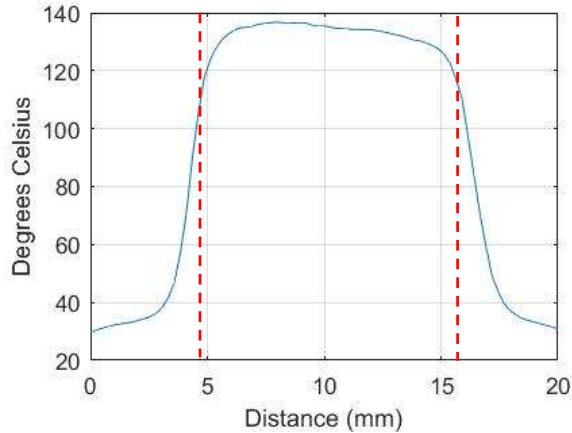


Figure 2.5 - Slice of temperature data for heating a square of powder. The temperature data for the middle row of the square of powder with a 100% radiation power step input after 4 seconds, the red dashed lines represent the edges on either side of the square. Two things to note here are the steep temperature gradients and asymmetry of the temperature distribution.

2.1.4 Melting and Crystallization

A differential scanning calorimetry (DSC) study [7] was referenced to guide selection of target sintering temperatures as well as the powder bed preheat temperature [10]. The DSC data in Figure 2.6 is for PA 2202 powder. This is the Nylon 12 powder used in thesis experiments and is produced by EOS. DSC measurements were obtained using a TA SDT Q600 in an air environment. This shows the melting phase transition starting at 175 °C and in cooling the crystallization begins at 155 °C. This suggests it would be desired for the powder to be heated as close to 175 °C as possible in the preheat without risking any areas overshooting, while the powder bed should be held well above 155 °C to delay crystallization until after the part is finished.

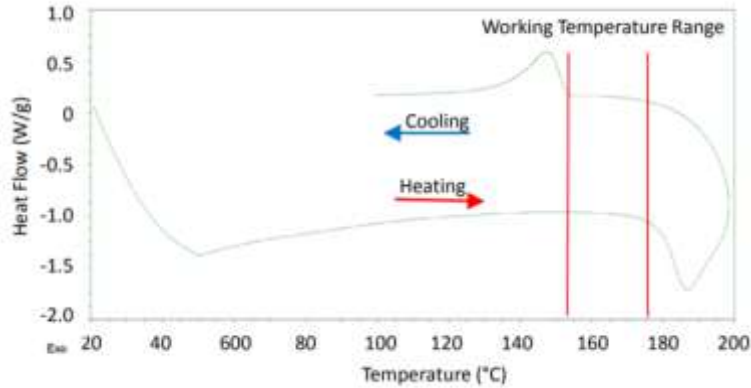


Figure 2.6 - DSC data for the Nylon 12 powder used. The melting phase transition begins at 175 °C and in cooling the crystallization begins at 155 °C. The powder was dehydrated in a roughing vacuum at 70 °C for 24 hours. [7]

2.1.5 Melt Pool Propagation

As the powder temperature increases beyond the melting point of 175 °C, the melt pool forms at the surface of the layer in the center of the sintering cross section. The melted polymer is a more effective conductor than the powder and further absorbed heat is conducted both outwards and downwards. As the cross section melts through the layer of powder, the lower part of the layer of powder switches from an insulator to a conductor, and the rest of the part (previously fused layers) acts as a heat sink.

As the melt pool approaches the corners (surrounded by unheated powder on three sides), the larger the temperature gradient and eventually the radiative heat input cannot overcome the rate of heat loss and the absolute tip of the corner is not sintered. The heat losses at a corner are readily seen in Figure 2.4. The higher the strength of a radiation source, the sharper of a temperature gradient it can sustain and thus the sharper features it can create and the shorter the sintering time can be.

For a uniform radiation flux it is clear that the interior points of a cross section will be heated faster than points closer to the edge. There are two potential advantages of closed loop temperature control here. First, the ability to keep the material within a working temperature window to potentially improve mechanical properties and/or avoid degradation. Second, there is an opportunity to prevent melt pool propagation beyond the boundaries of the cross section in areas that would have been overheated in open loop control.

CHAPTER 3: SYSTEM HARDWARE DESIGN

In order to explore the independent and dependent variables involved in LAS cross section resolution, a test platform was designed to create a controllable and repeatable environment for experiments to be conducted. This chapter explores the requirements of the test platform and how these were met from a hardware standpoint. The suppliers & P/N's of critical parts are listed in Appendix A.

3.1 System Overview

The test platform used had to create a repeatable, controlled environment for sintering (see Figure 3.1). To reduce convection cooling to the powder bed, it was to be enclosed in an insulated build chamber with an elevated ambient temperature. The powder bed itself had to be thermally controlled via radiation and conduction, as well as mechanically actuated to travel linearly within the build chamber. To produce consistent thickness layers, a layer deposition mechanism was required. Finally hardware had to be implemented to allow thermal observation of the sintering area, while additional hardware was required in order to control the system mechanically and control the projector.

The enclosed build chamber had quartz glass on top at one side with the projector mounted directly overhead of this glass. This was the sintering side of the build chamber, and the opposite side was for powder deposition. After a new layer was deposited on the layer deposition side, the powder bed was moved to the sintering side and the layer was sintered, then moved back and the process was repeated. There was a hole in the side at the sintering end of the build chamber in

order for the thermal camera to capture the sintering process. Two computers were used to control the movement / heaters and the projector, respectively.

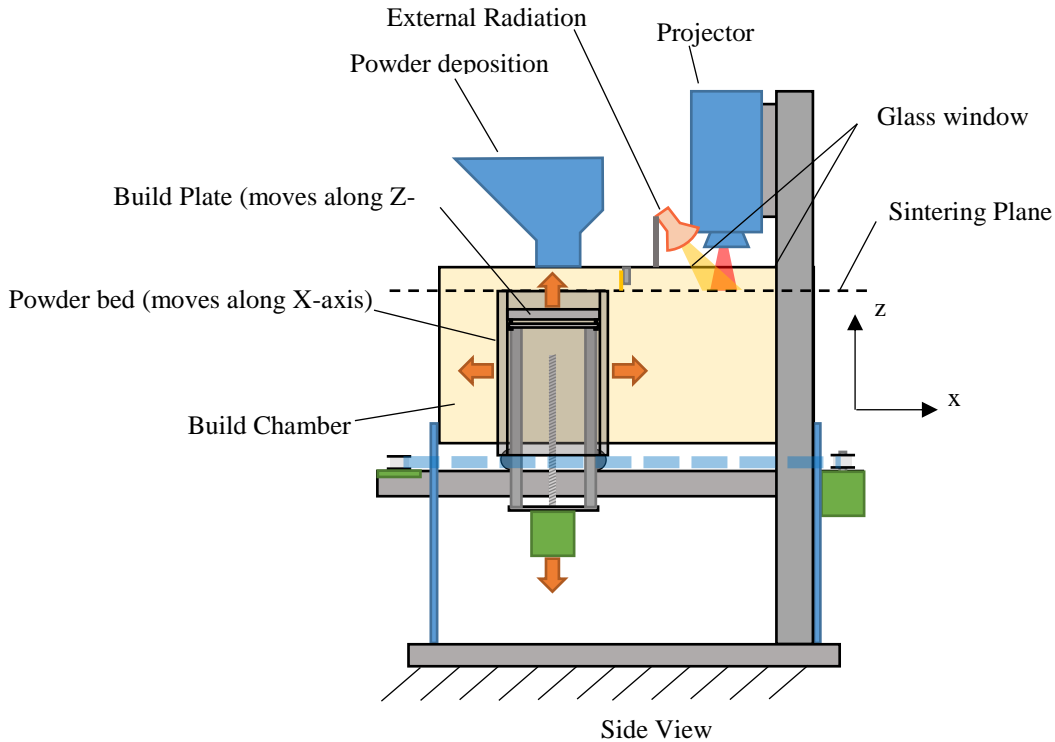


Figure 3.1 - A schematic of the full system. Layer deposition occurs at the left, the powder bed then moves to the right (along the positive X-axis) for the layer to be sintered, and the process repeats.

3.2 Build Chamber / System Chassis

The build chamber was a rectangular prism enclosed with insulation. The long dimension represented the X-axis, along which the powder bed moved inside of the build chamber. The Z-axis was the vertical direction along which the build plate moved when new layers were spread. The build plate dropped one layer thickness for every new layer deposited (user selectable, but usually 100 microns), which represented movement in the negative Z-direction. The coordinate system used to refer to these axes is right handed which gives the direction of the Y-axis.

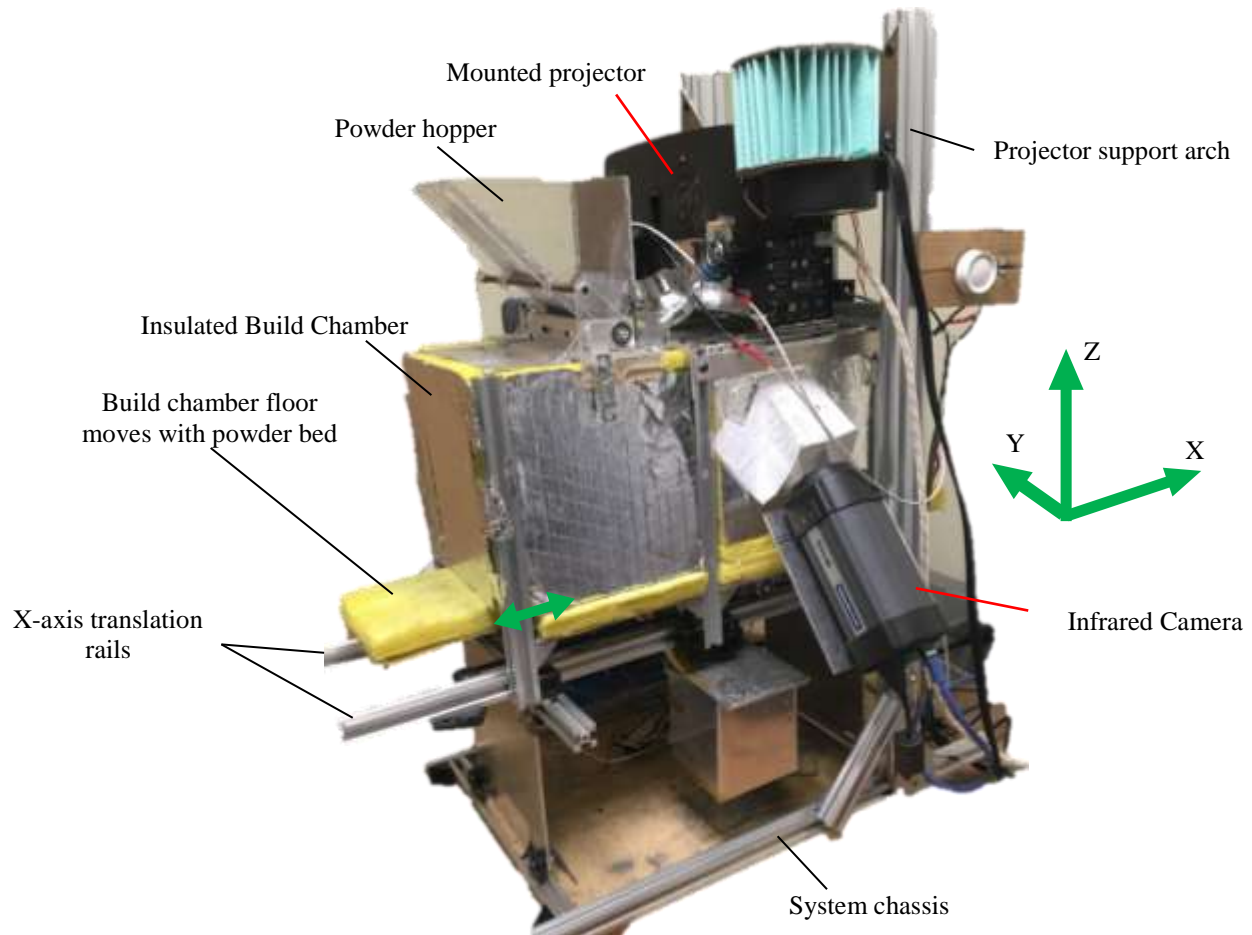


Figure 3.2 - An isometric view of the full system. The build chamber floor moves with the powder bed and therefore protrudes from one side of the other at any given time – this allows fewer and tighter air gaps to keep more heat in.

The main material used to construct the system body was V-Slot Linear Rail ®. This is a 20 x 20 mm cross section 6061 aluminum rail with a slot extending down each of the 4 sides accepting low profile M5 nuts to readily mount hardware. In order to contain the heat, 1” thick fiberglass insulation was used to enclose the build chamber. The interior dimensions of the build chamber were 37 cm long x 17 cm wide x 17.5 cm tall). This allowed the powder bed a 200 mm range of travel on the X-axis.

A final part of the chassis was the projector mounting frame. This extended from the chassis base above the build chamber then had two connecting pieces that the projector bracket was

mounted to. This bracket allowed the projector to be pivoted about the Y-axis to make sure the image focus plane was parallel to the powder surface. This frame positioned the projector over the quartz glass at the top of the sintering end of the build chamber, with the powder surface 60 mm from the projector lens.

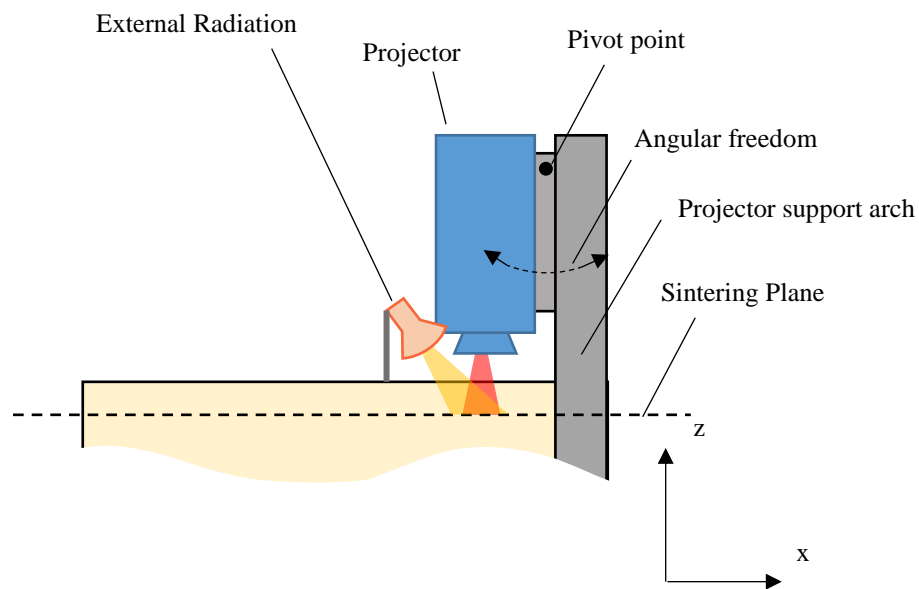


Figure 3.3 – Projector mounting on a pivoting bracket. The projector was mounted on a pivoting bracket such that the image focus plane (60 mm from lens) could be adjusted to align with the layer sintering plane. The projector support arch was rigidly mounted to the chassis, the calibration could be compromised by as little as 250 microns of projector movement (the size of one infrared camera pixel on the print bed) in the X-Y plane.

3.3 Powder Bed

3.3.1 Components / Construction

Because the powder bed was to be heated, only components that were capable of withstanding temperatures of greater than 200 °C were used. The powder bed walls consisted of a 6061 aluminum square tube oriented vertically, with a build plate within them (see figure). The aluminum square tubing was 4" x 4" with a 1/4" wall thickness leaving the interior dimensions at 3.5" x 3.5". Two aluminum plates on either side of the powder bed extended through slots in the

build chamber floor, with wheels mounted on PEEK plastic spacer brackets to insulate the bearings from the heated powder bed. These wheels rolled on rails mounted in the X-direction to allow X-axis motion of the powder bed.

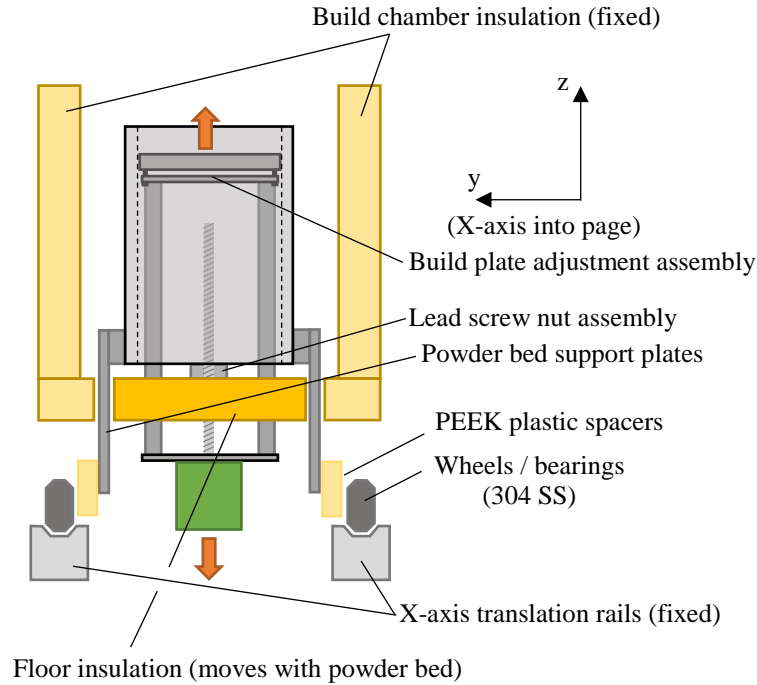


Figure 3.4 - End on view of the powder bed (movement into and out of the page). The bed rolled on 304 SS wheels in grooves on X-axis translation rails, constraining it to one degree of freedom.

The build plate was made from 3/8" thick 6061 aluminum and cut to fit with tight clearance within the aluminum square tubing (target gap 250 μm). A 1/8" fiberglass rope gasket fit into a groove to create a seal against the wall to prevent powder leakage. High temperature silicone caulking was used to adhere the gasket to the groove around the build plate's circumference. The build plate support assembly included 4 screws, two supporting the build plate in compression and two securing the build plate in tension. By adjusting these the build plate could be leveled relative to the support assembly.

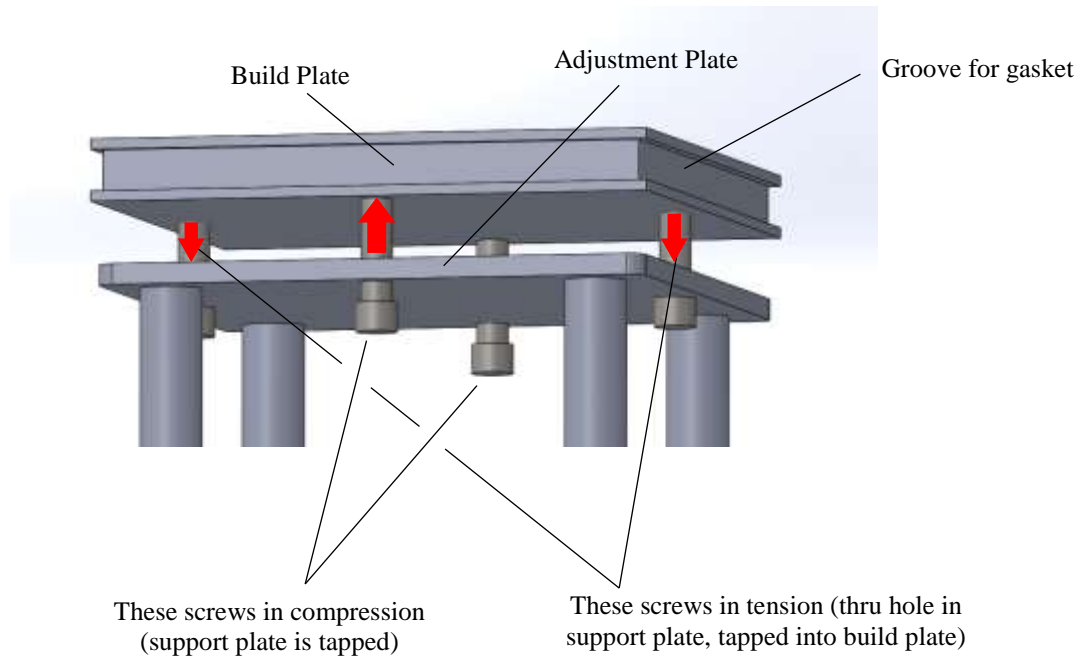


Figure 3.5 - The build plate adjustment assembly. This allowed the plate to be leveled in relation to the powder bed. This was accomplished using four M3 machine screws, two pushing up on the build plate and two pulling down in tension.

The build plate sat on a support assembly composed of two plates with four aluminum posts separating them. The lower plate had a stepper motor mounted to it. The stepper motor drove a lead screw which suspended the entire assembly from a lead screw nut on a cross bar connected to the base of the square aluminum tubing (see figure). This assembly allowed for the movement of the build plate in the Z-direction as new layers were spread.

3.3.2 Mechanical Control

The X-axis motion of the powder bed was driven by a stepper motor mounted to the chassis with a timing pulley and timing belt. The build plate motion in the Z-direction was driven by a lead screw and stepper motor. The control of these motors is addressed in 3.7 Control Hardware.

3.3.3 Thermal Control

Both conduction heating and radiation heating were used to heat the powder bed. The bulk temperature of the powder was heated mostly through conduction with strip heaters lining the base and walls of the powder bed. The surface temperature of the powder was heated predominantly via radiation. The control of these heating zones is addressed in 3.7 Control Hardware.

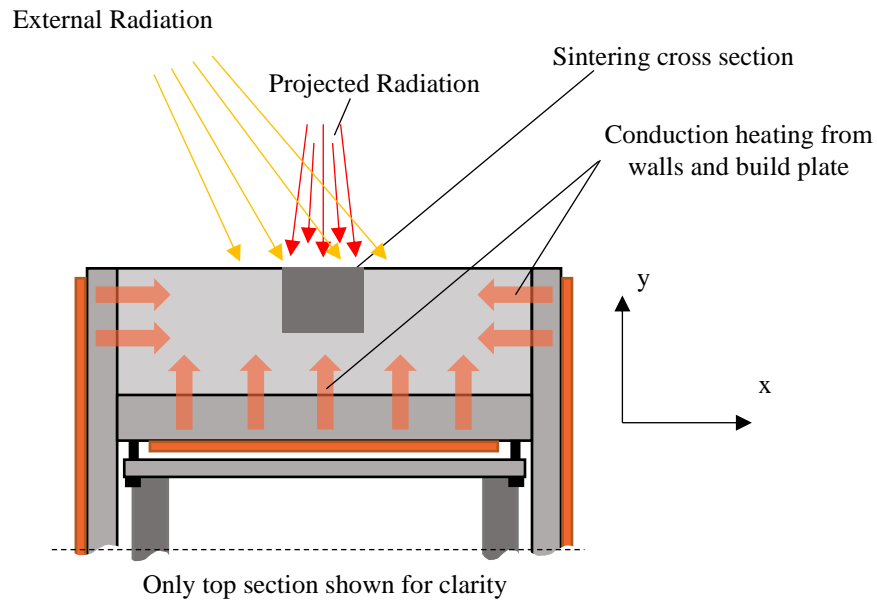


Figure 3.6 - The methods of powder bed heating. The powder bed was heated from the sides and bottom via conduction. The powder surface had an external halogen lamp to heat the full surface area of the powder (only necessary as powder bed depth increased), with the concentrated projector radiation for sintering patterned cross sections.

3.3.3.1 Powder Bed Bulk Heating

There were two zones of conduction heating in the powder bed: the walls and the build plate, both having closed loop temperature control. Each wall of the powder bed had a 120 V (AC power) 90 watt 3" x 3" strip heater, with a 100 k Ω thermistor embedded within the wall. The build plate had a 120 V AC power 90 watt 3" x 3" strip heater underneath it, with a 100 k Ω thermistor for temperature embedded in center of the plate. Aluminum was an ideal material as it has a high thermal conductivity which allowed for minimal thermal gradients for a given heat flux.

A benefit of this was the ability to control the cooling rates and recrystallization of the parts within the powder bed, and it reduced thermal gradients in the XY plane of the sintering layer by increasing the temperature of the bulk powder in the powder bed. Additional external radiation besides the projector played a more significant role in heating the top layer of powder. This is discussed later.

3.3.3.2 Powder Surface Heating

The powder surface temperature was actively controlled via two methods: external radiation from a 60 Watt halogen lamp and the projector radiation itself. The halogen was a 10° bulb connected to a mechanical dimmer switch, and it was rarely increased to over 10%. In early layers, this extra radiation was not necessary as the powder bed was so shallow the build plate heating from below was sufficient. However, thicker parts require the additional external radiation to maintain an elevated surface temperature. For example, with the build plate heater set to 176 °C and a powder bed depth of 500 microns, the powder surface temperature without external radiation was 165 °C. When the powder bed depth increased to 2 mm the surface temperature without external radiation was 140 °C. This is where the external radiation became more important.

3.4 Layer Deposition

3.4.1 Powder Deposition

The layer deposition system was composed of two main components (seen in Figure 3.7) which acted in tandem with the system's ability to move the powder bed along the X-axis. There was a powder dispensing assembly which deposited powder onto the powder bed as the powder bed moved underneath in the positive x-direction and a smoothing assembly to distribute this powder into flat and thin layers.

The powder dispensing assembly involved a powder hopper placed above a grooved drum which was sealed against a spring loaded nylon gasket. As the drum spun while immersed in powder the grooves were filled and after passing the nylon flange dropped their contents onto the powder bed. In this way finite amounts of powder was placed on the powder bed for the spreader to smooth flat. For 100 micron layers, two grooves worth of powder were enough to cover the whole build plate with a full layer of powder.

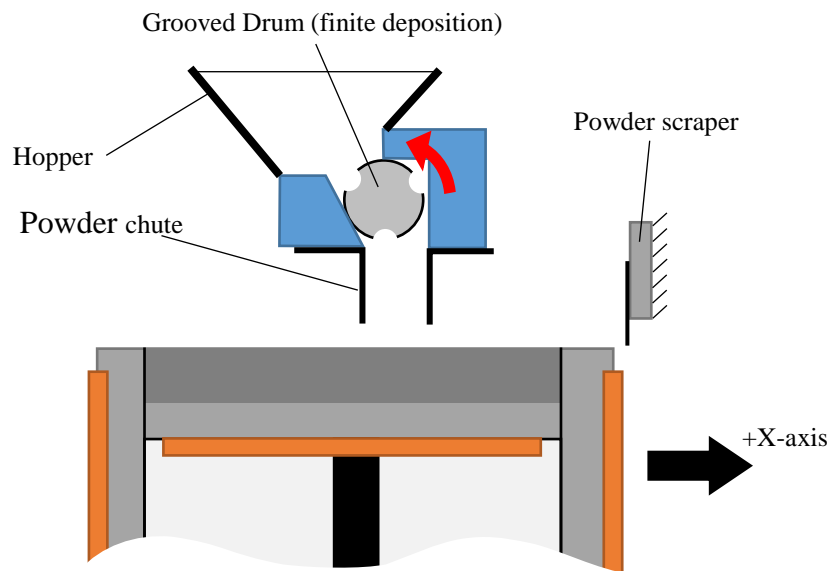


Figure 3.7 - The layer deposition system provided consistent layers. This was made up of a grooved drum that rotated to deposit powder, and a powder scraper to spread the powder into a uniform thickness layer. The trial layers in all experiments were 100 microns thick.

3.4.2 Powder Layer Spreading

The system had the ability to use either a powder scraper or a powder roller to spread the deposited powder. The powder scraper was a glass slide mounted to an aluminum bar which was fixed to the chassis of the machine. The scraper was oriented perpendicular to the powder bed surface as well as perpendicular to the motion of the powder bed on the X-axis (parallel to the YZ plane). Movement of the powder bed in the positive x-direction passed it under the scraper which

left a clean flat layer of fresh powder. The powder roller was a polished 304 stainless steel rod, 5/8” in diameter, driven in a direction so the side closest to the powder bed was moving opposite of the powder bed’s motion in the positive X-direction (counter rotating). This was driven at approximately 150 RPM, and was shown in prior testing to produce denser powder layers than the scraper (by about 10%). An added bonus was that the powder roller heated up to the ambient temperature of the build chamber, and helped to preheat the top layer of powder as it was spread.

As the bed moved under the scraper /roller, powder built up in front and also spilled over the sides of the powder bed. For this reason an aluminum sheet metal gutter system was installed which drained to a reservoir below the powder bed. This reservoir was in ambient temperature as powder degrades more at elevated temperatures. In this study a glass powder scraper was used for simplicity as well as lack of availability of a tight tolerance roller. Runout of the machined roller was too high to create consistent flat layers.

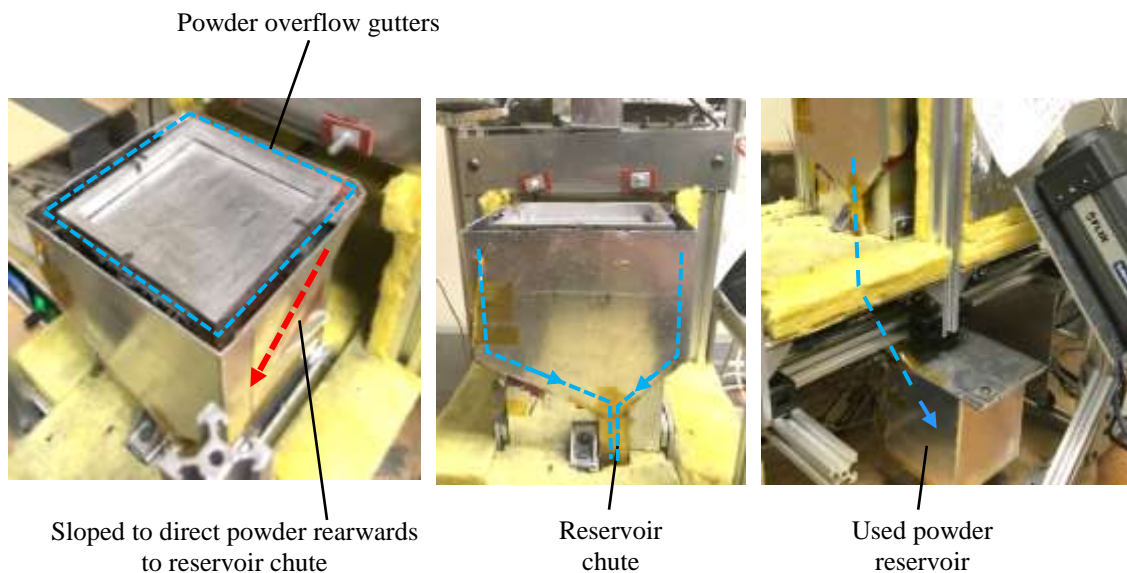


Figure 3.8 - The powder overflow gutters. These served to prevent powder spillage around the powder bed and gave the ability to store lightly heated powder in a low temperature reservoir. Only fresh powder was used for experimentation.

3.5 Projector

3.5.1 Models Used

The first projector used in this experiment was an Optoma X341. This projector had a resolution of 1024 x 768 pixels and an advertised brightness of 3300 lumens off the shelf [11]. After finding the optics had become dirty, this was exchanged for the nearly identical Optoma X316, which has an advertised 3200 lumens [12].

Table 3-1 Optoma X316 projector specifications. These are identical to the X341 specifications aside from a very slight change in optics, leading to a slightly higher lumen output in the X341 (3300 vs 3200 lumens). Because the front lens was removed, the optical specifications no longer apply and are omitted. [12]

Optoma X316 projector specifications (off the shelf)	
Display Technology	Single 0.55" XGA DC3 DMD chip DLP® Technology by Texas Instruments
Resolution	XGA 1024 x 768
Brightness (no modifications)	3200 ANSI Lumens
Contrast Ratio	20,000:1
Lamp Life ² Bright	5000 (hrs)
Dimensions (W x H x D)	12.4" X 8.8" X 4"
Aspect Ratio	4:3 Native, 16:9 Compatible
Uniformity	80%
Horizontal Scan Rate	15.3 - 91.1kHz
Vertical Scan Rate	24 - 85Hz
Power Supply	100-240V, 50-60Hz
Power Consumption	225W Bright mode / 191W Eco mode (< 0.5W Standby)
Lamp Type	190W

3.5.2 Modifications Made

Both projectors were modified in the same way, except the latter had a HEPA filter installed on the intake blower, with the power increased to create positive pressure within the system. In order to get more power from the projector the color wheel was removed, which meant the light was shining onto the DMD (digital micromirror device) at full intensity instead of having

certain wavelengths filtered out at any given time. With this additional radiation on the DMD and also the orientation change of the projector, it overheated more easily (there is a temperature alarm on the DLP chip), so additional convection cooling was added. This is illustrated in the figure below.

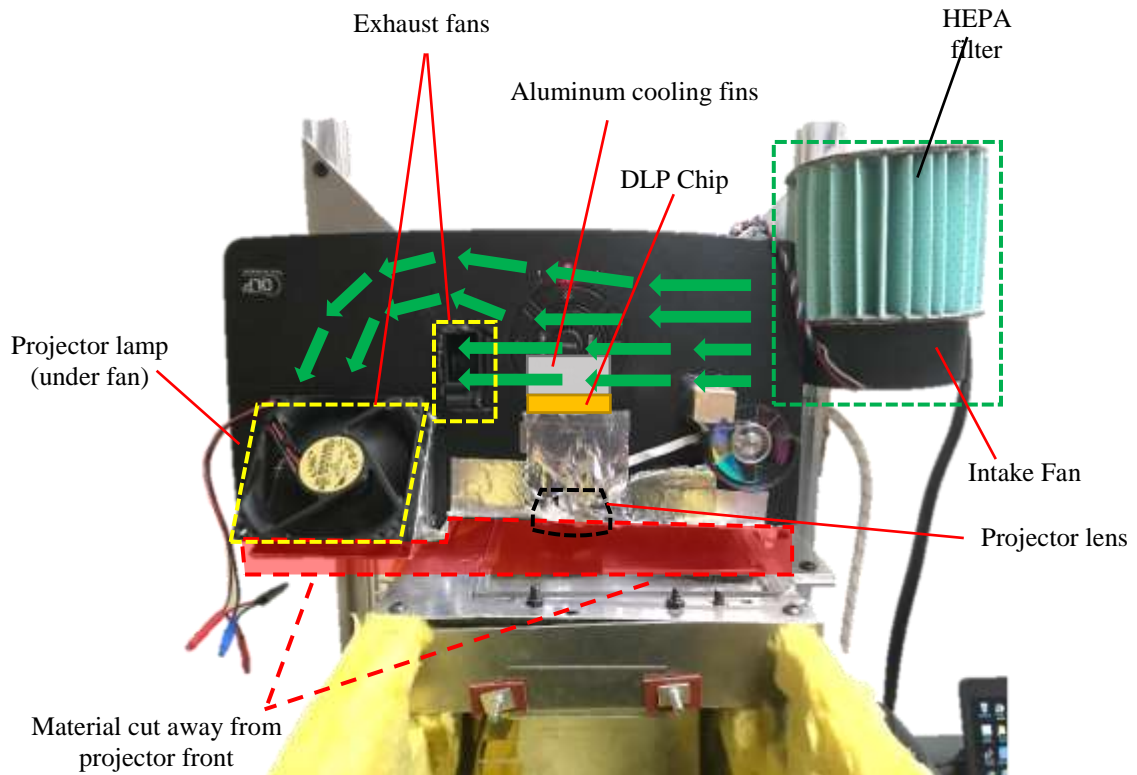


Figure 3.9 – The projector modifications. The front face of the projector was cut back to allow it to fit appropriately into the system. A centrifugal fan with a HEPA filter was the only intake for airflow and two exhaust fans ensured the airflow passed over critical components (the DLP chip and the projector lamp). Positive pressure was maintained by increasing the power of the intake fan, reducing the chance of foreign object debris / contamination of the interior optics.

When it was discovered that the initial projector’s optics had been fouled in some way, multiple precautions were taken on the second projector. In the prior assembly there was negative air pressure in the projector, no filtration on the intake blower, and the internal optics that weren’t hermetically sealed (mainly the light pipe leading up to optics) were exposed to open air. In order to reduce the likelihood of this happening on the next projector the first step was to seal off all

openings except for distinct inlet and outlet areas, leaving a tightly fitting ring for the projector's front lens to fit through. A HEPA filter was made by modifying a HEPA vacuum filter and fixed to the blower intake, and the blower was dialed up to a power high enough to create positive pressure within the projector body. The filtered intake and positive pressure made it much more challenging for any particles to enter and foul the projector optics.

The outermost lens on the projector as it is supplied from the manufacturer is used as a focusing lens, which is adjustable and allows the user to focus the image at a distance on the order of 5 meters. This projector was chosen largely because when this lens is removed, the projected image becomes focused at a distance of 60 mm. This focused image measures 21 mm wide (in the Y-direction) and 16 mm tall (in the X-direction). Each time the light passes through a lens it loses power, so an additional bonus of removing this focusing lens is an increase in radiation energy available.

With the projected image focused so close it was necessary to cut away most of the plastic housing around the projector, to make room for the heated build chamber surrounding the powder bed. Figure 3.9 shows this modified structure. The projector comes programmed to not function unless the color wheel is spinning, so when the color wheel was removed from the light path it was kept attached and mounted to the frame so it could spin freely.

3.6 Thermal Camera

Observing the sintering process from a thermal standpoint proved to be challenging for a number of reasons. In order to preserve the thermal camera, it had to be mounted somewhere outside of the build chamber in ambient air temperature. This meant it was either going to be looking through a window, or a hole in the insulation. The issue with the window is that it takes a very expensive (~\$75,000) medium wave infrared camera in order to see through quartz glass, and

this is true of all materials that are transparent in the visible range with minimal losses. The long wave infrared camera purchased for this experiment was an order of magnitude cheaper however was not able to see through the glass window at the top of the system that the projector shined through. This meant that there was no option but to have a hole in the insulation for the infrared camera to look through. Because of the projector and powder hopper there was no room above for the camera to be mounted, and the best solution turned out to be mounting the camera to the side and looking at the sintering area via a polished aluminum mirror. This mirror was ordered as 1/8” pre polished aluminum (#8 mirror finish) which was then polished down further by hand using 6 micron polishing solution.

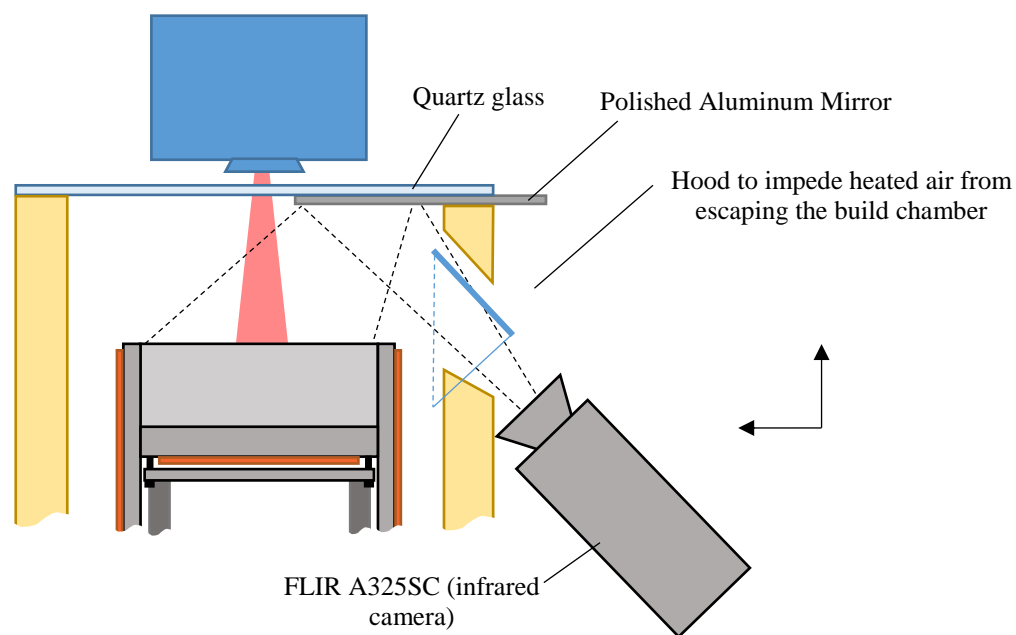


Figure 3.10 - The infrared camera orientation. The long wave thermal camera was unable to view radiation transmitted through the glass; a mirror was found to effectively reflect the infrared radiation for the camera to capture. A hood over the hole in the insulation helped to prevent heated air from escaping the build chamber.

This thermal camera arrangement meant there had to be a hole in the side of the insulation, so in order to minimize heat losses a hood was placed over the hole, loosely fitted around the

thermal camera to allow airflow. Because the camera was observing the sintering area off of a mirror at an angle, the resulting image was distorted and also flipped. This meant that a calibration step was required in order to relate a pixel in the thermal image to the reference frame of the sintering image. This is discussed in detail in chapter 4.

3.7 Control Hardware

For all motion control and also conduction heating of the powder bed, the system used a RAMPS 1.4 controller board (commonly used to control RepRap 3D printers). This board was a shield for the Arduino Mega. When combined with Marlin (firmware), the board can be communicated with using Repetier (software) as a GUI. The controller board was housed in a control box with the associated additional hardware for temperature control.

A computer running Repetier was used to communicate with the controller board to give it the motion and temperature control commands. With the requirement that MATLAB was in an infinite loop while sintering layers with key press commands to start new layers, it was best to use a separate and more powerful computer to run the main sintering script and communicate with the projector and the thermal camera.

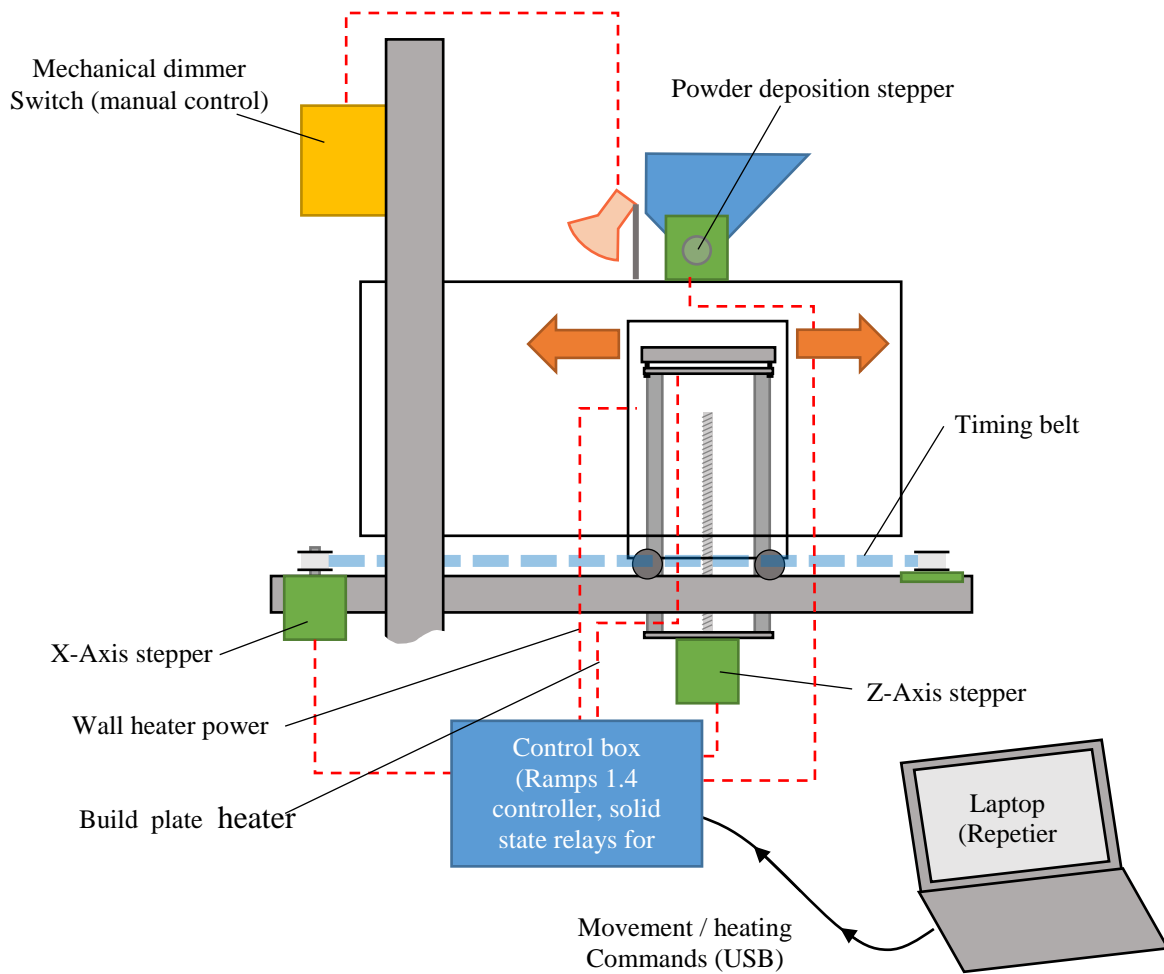


Figure 3.11- A schematic of the physical control of the system. The control box was a central hub for this control, and a computer running Repetier sent the Ramps 1.4 controller board control commands via USB.

The Repetier software sends commands to the RAMPS controller board using G-code. The board then deciphers these commands and sends the necessary signals and power to the stepper motors to power the motors to the correct displacement. The calibration between linear distance traveled and the G-code displacement command was located in the Marlin firmware (uploaded to the Arduino Mega). Calipers were used over large displacements (> 10 cm) to achieve accurate calibration constants which related motor steps to axis translation in mm.

There were three stepper motors on the system. One stepper motor drove the X-axis timing belt, another drove the Z-axis lead screw, and a third rotated the powder deposition grooved drum.

3.7.1 Temperature Control

Both conduction heating zones (walls and build plate) were wired to solid state relays to power them, with the control module actuating the relays. The Marlin firmware uploaded to the Ramps control module uses PID control adapted for relays.

The external radiation halogen is controlled by a mechanical dimmer switch. This was manually controlled and therefore for thin parts where it was not necessary, was left off during trial layers for improved repeatability.

3.7.2 Projector Control

The projector was connected via HDMI as a second monitor to a laptop, and the thermal camera was interfaced with using MATLAB on that laptop. MATLAB was used to generate the images displayed to the projector which were then displayed using the Cogent toolbox, this process is discussed in detail later.

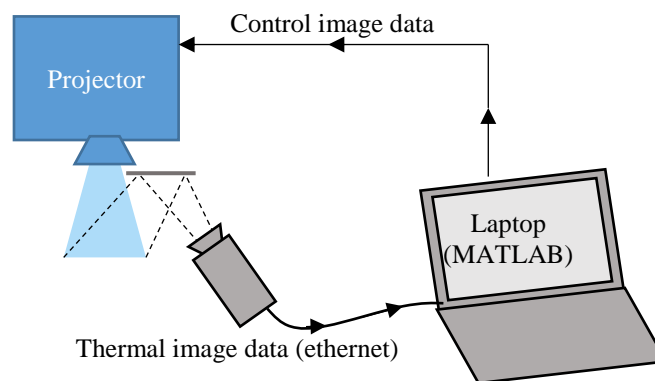


Figure 3.12 – The feedback control layout. The computer running MATLAB had the ability to capture the thermal data from the sintering process and in the case of closed loop control use this thermal feedback to implement negative feedback control.

CHAPTER 4: SYSTEM CONTROL

In the first generation system mentioned earlier, timed exposures of a constant radiation pattern were projected onto a heated powder bed to sinter layers in a simple implementation of LAS [7]. This is considered open loop control in this experiment, when the radiation pattern and intensity does not change for the duration of the sintering of a layer. This system hosts many improvements over this previous implementation, most significantly an integrated infrared camera enabling closed loop control and temperature monitoring of the surface powder.

The infrared camera allowed the use of closed loop temperature control of the sintering of a layer. In closed loop control MATLAB was used to read this data and process it, and the resulting output was the image containing the cross section radiation pattern and intensity profile. This characterized the amount of radiation that would be exposed by each pixel from the projector. The preliminary challenge was mapping from the thermal camera pixel positions to the associated pixel positions in the projector reference frame. A calibration step was required to generate this mapping. With the positional relationship solved, the temperature data then had to be run through a control algorithm and the resulting new radiation intensity profile sent to the projector. In order to quantify the benefits of closed loop control, open loop control had to be tested as well, which only required a simple modification of the closed loop control architecture already in place.

4.1 Motivation for Closed Loop Control

In preliminary experiments, with all of the sintering area at full intensity, it was observed that the inner parts of the sintering cross section heated up the fastest and melted first. This melt

pool then spread outward towards the edges and corners. The central areas sometimes reached over 215 °C (this was cross section dependent) in this time. Given this behavior of the melt pool being heated well beyond the plastic’s melting temperature (175 °C), there was an opportunity for the melt pool to overshoot the desired cross section and finish larger than intended.

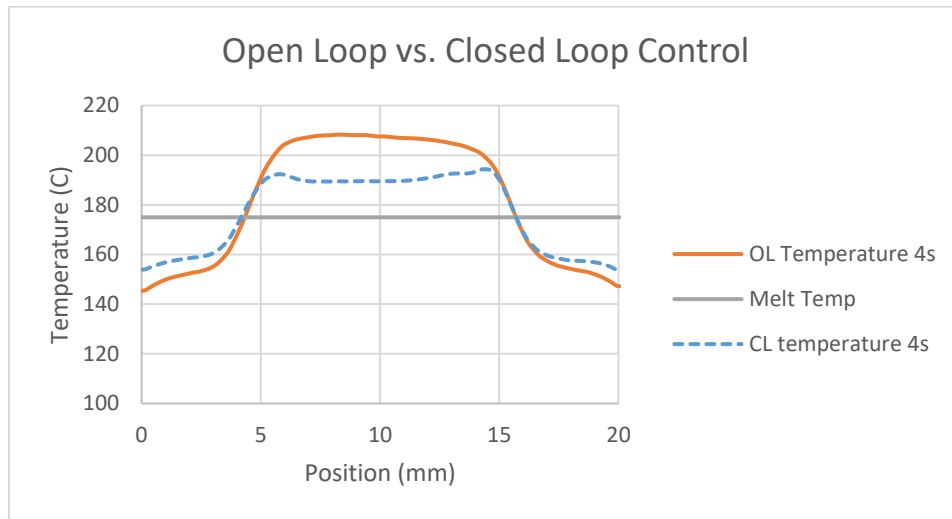


Figure 4.1 - The temperature distribution across a 12mm circular sintering cross section. This was in a preliminary experiment, and the closed loop temperature target was 195 °C, and the overheating was substantially reduced as a result of this.

4.2 Characterization of Projected Radiation

The projected radiation was characterized by the radiation pattern and the radiation intensity profile. The radiation pattern was the geometrical shape of the radiation projected onto the powder bed, and was identical to the desired sintered cross section for all trials in this experiment. The radiation intensity profile was the main independent variable for the trials. For open loop control the intensity across the radiation pattern was constant (100% unless otherwise noted). In closed loop control, the intensity profile was calculated according to the real-time temperature distribution of the sintering cross section, with more radiation being sent to the areas that were farther from the target temperature.

The emitted radiation pattern and its associated intensity profile were governed exclusively by the image sent to the projector. The outline of the image matched the target radiation pattern. The shading of the area within the pattern was directly correlated with the radiation intensity profile. This was implemented in the form of a grayscale, with 0% power corresponding to the color black, and 100% power corresponding to a fully white pixel on the image. MATLAB was used with a grayscale color map to take a control signal from 0 to 1 and output the corresponding black / white / shade of gray in between. This was not linear, which is considered in 4.5 *gray scale calibration*. All parts in this thesis were of constant cross section throughout the layers. Figure 4.2 shows a cross section image and the part that resulted from it.

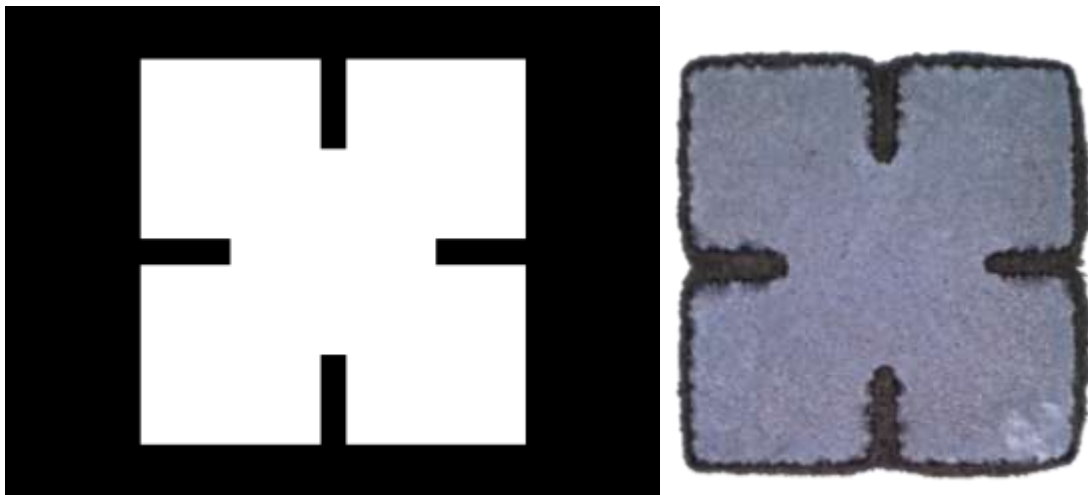


Figure 4.2 - Cross section reference image (left) with resulting sintered part (right).

4.3 Geometric Calibration

Before any control algorithm was applied to generate the projected image, accurate temperature data for the sintering cross section was required. In order to account for the distorted thermal image, the thermal image coordinate system had to be mapped to the projector reference frame, the projector reference frame being the projected image on the powder bed. This was done in two steps. First, the full frame infrared camera image was mapped such that the quadrilateral

shape of the sintering area outline (infrared camera reference frame) was “stretched” to fit a 60 x 80 pixel area, with the new pixels being assigned values via interpolation (this is done using MATLAB’s `imwarp` function). This warped the entire image, but only the sintering area was of interest so this area was cropped as the second step from the much larger print bed thermal image to give a 3:4 aspect ratio 60 x 80 pixel image of the sintering area.

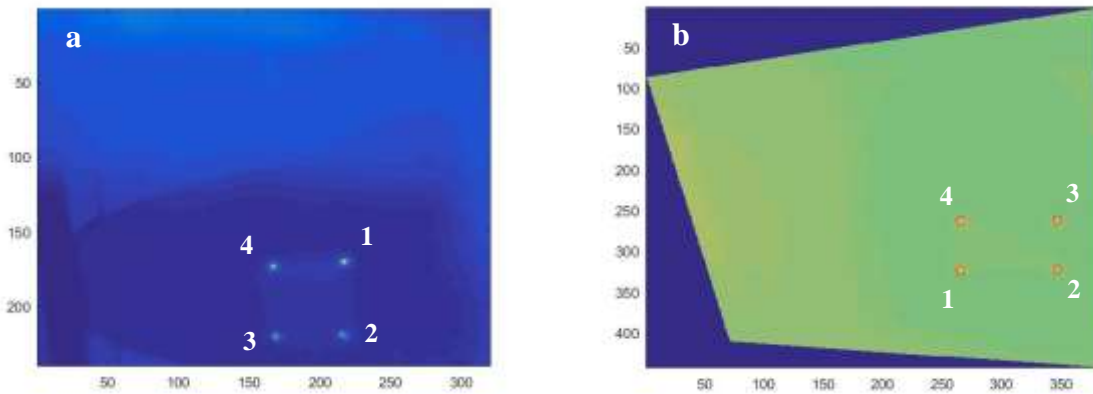


Figure 4.3 – The geometric calibration. The full frame thermal camera image a) is linearly distorted to create b) the image on the right. These points are from the calibration step and represent the four corners of the projected image. Note that in the transformation the image is not only stretched but also transposed, with corners 1 and 3 flipping. This image on the right is then cropped to size. The color change in the image to the right is explained by the autoscale color mapping in MATLAB, because the warped matrix fills in the new area with 0’s it registers as “cold” and makes the rest of the screen look more moderate, the impact is only cosmetic.

4.3.1 *Warping the Thermal Image*

It proved simplest to use known points in each reference frame and MATLAB functions to relate them. This was done in the calibration script. The first challenge was to identify the four corners of the projector reference frame, also known as the sintering area. In order to do this, room temperature powder was spread and four squares of white light at full power were projected onto the powder bed in the four corners of the projected image. These squares were 30 x 30 pixels (projector reference frame), or roughly 600 x 600 microns. The squares were left on for 5 seconds

and then a thermal image was captured, resulting in a thermal image of the powder bed with 4 distinct heated areas representing the 4 corners of the projected area (shown in Figure 4.3).

In the thermal camera reference frame, because of the image being flipped across the mirror and rotated 90 degrees, the points had to be correctly associated in each reference frame in order to warp the image correctly. In Figure 4.3 the points are labeled 1 – 4 and it is seen that as a result of the rotation and flipping the points are transposed from Figure 4.3a to Figure 4.3b.

The image was displayed and using `impixel()` MATLAB tracked the row and column of 4 user clicks corresponding to the 4 corners of the sintering area. The order that the points were entered had to correspond with the point index, so the points were clicked sequentially from 1 – 4.

Table 4-1 Thermal camera calibration.

Thermal camera image (Figure 4.3a)		Warped / transposed image (Figure 4.3b)	
Point index	Position on image	Point index	Position on image
1	Upper right	1	Lower left
2	Lower right	2	Lower right
3	Lower left	3	Upper right
4	Upper left	4	Upper left

To eliminate human error, the script used these corners as a reference and searched for the hottest pixel within a 10 pixel radius of the user’s click for each of the four points. These new points represented the center of the projected dots, for which the location in the projector reference frame was also known (for a 30 pixel square the center would be 15 pixels from each edge of the projector reference frame for every corner). The MATLAB function `maketform('projective', [c2 r2], [c1 r1])` takes four observed points in the thermal image `[c2 r2]` and four known locations of the points in the projector reference frame

[c1 r1] in the form of row and column arrays and gives a transformation. The [c1 r1] data is hard coded into the script as it does not change, and the order corresponded to the point indices as shown in the table. The resulting transformation matrix that came from `maketform` (with an intermediate step involving $T = \text{tform.tdata.T}$) was then plugged into `projective2d(T)`, a function whose result was directly put into `imwarp(image, transform)` which transformed the thermal image to the new mapped image.

4.3.2 *Cropping the Warped Thermal Image*

This gave a new image where the sintering area was a rectangular 80 x 60 pixels, but this was only a small portion of a much larger now warped image. Continuing with the calibration steps, this warped image was displayed to the screen and using `impixel()` the four corners were chosen again to crop the image down to just the projected image area. This was done using the same method as before where `impixel()` was used to track where the user clicked on the MATLAB image displayed, then the hottest pixel within a 10 pixel radius of each point was taken to represent the position of that point. For each corner this position was then offset by half the width of the heated square in each direction to represent the true corner of the projected image. Other methods were attempted where a temperature weighted average was taken to get the exact position of the points but they proved less effective.

4.3.3 *Configuration File*

At the start of every experimental trial the MATLAB script opened a configuration file which contained the thermal image transformation constants as well as the control gains and sintering parameters. By separating this from the script it was easy to quickly change values between trials. Below is an example of the configuration file for a trial. Instead of writing an

additional script to implement open loop control, the temperature target was simply set to a value so high the control signal was guaranteed to be saturated. With the temperature target at 500 the error was always so large that this was accomplished, and the radiation profile was at a constant 100% power.

```
t_matrix % this matrix defines the linear warping of the image
  0.0745   1.0143   0.0006
  1.2802  -0.0427  -0.0014
 -231.6979 -160.1663   1.0000
kp ki kd % control gains
30 0 0
Sintering Time % total time sintering layer is exposed (seconds)
4
Temperature Target % the reference temperature used as the target in closed loop control
500
c3 % the columns defining the cropped rectangle from the warped image
233 313 313 233
r3 % the rows defining the cropped rectangle from the warped image
313 313 253 253
```

Figure 4.4 - An example configuration file. This contains the transformation matrix for thermal image mapping, the control gains, the target sintering temperature, and the cropping coordinates to crop the projected image area from the warped thermal image.

This was the final step of the calibration, and a configuration file was created to log the transformation matrix as well as the cropping points. The full code for this is in the appendix.

4.3.4 Calibration Accuracy

The size of a thermal image pixel on the print bed varies slightly as it is viewing the print bed from an angle, and vertical direction in the thermal camera reference frame corresponds to the horizontal direction of the projector reference frame. The projected image (average dimensions) was observed to be roughly a 50 x 50 pixel area of the thermal image. Because the projected image was 21.5 mm wide x 16.1 mm tall, each thermal pixel represents a 430 micron wide x 320 micron tall area on the projected image. To contrast this, the 1024 x 768 projector resolution makes each

pixel on the print bed 19.5 x 19.5 microns, 15 – 20 x smaller than what the thermal camera can resolve depending on the direction.

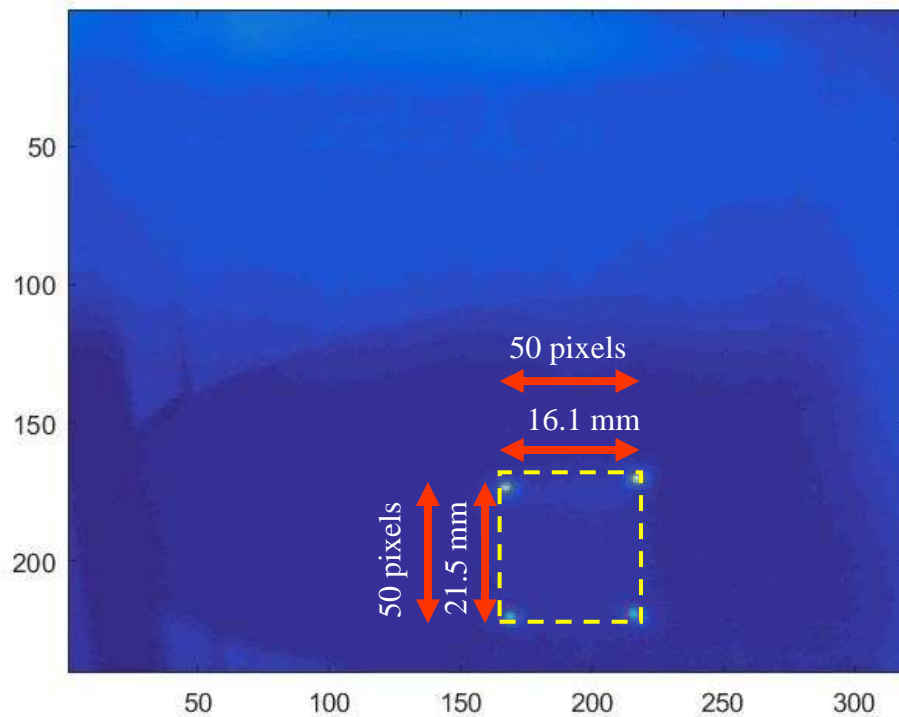


Figure 4.5 - The resolution of the thermal camera. This is given by the ratio of thermal image pixels to the corresponding distance on the print bed. In the vertical direction of the projected area the 50 pixel length covers 16.1 mm, this corresponds to a ~320 micron pixel length, in the horizontal direction this is roughly 430 microns.

The effect of a thermal pixel that falls half on and half off of an area that is receiving radiation is that the temperature would be averaged, and the edge would register at a lower temperature because of the cool powder contributing to the temperature average. This all means that the calibration can only be trusted to be accurate to within 430 microns as the pixels are used to set the calibration. An algorithm that took a temperature weighted position average for the points was attempted but proved to give worse results than using the point that registered the maximum temperature. Imperfections in the mirror polishing / FOD (foreign object debris) on the mirror and

thermal camera lens are two other factors that while controlled to the best ability, could have further affected the calibration (successful calibrations were run so these effects were considered negligible for the given resolution).

4.4 Control Architecture

With the temperature data mapped to the projector reference frame the software had to take this data and generate a control signal. In software implementation there were two critical images for each sintered layer, the reference image and the control signal image. The reference image was a black and white image of the target cross section, saved as a 256 color bitmap; this defined the radiation pattern (the shape of the sintering cross section). In this image the cross section / radiation pattern was white with all other pixels black. The control signal image was a grayscale image of the same pattern with the interior shading a function of the local temperature, calculated by the control algorithm.

4.4.1 Choosing a Processing Resolution

A resolution had to be chosen for the image processing, with the value added and the cost of higher resolutions considered. Higher image resolution at the projector would lead to sharper lines and features in the projected radiation. The cost of this higher resolution is longer processing loop time. Keeping in mind that a projector pixel was 21 x 21 microns, the native resolution of 1024 x 768 was abandoned for a 512 x 384 pixel resolution. This is justified as the powder particles were at a minimum 30 microns and it would not be realistic to melt only part of a particle. The resulting control loop time reduction was significant, dropping from an average of 300 milliseconds to an average of 170 milliseconds.

4.4.2 *Generating the Control Signal*

The temperature data was resized and the reference image used to generate a target temperature matrix, these then were subtracted to generate a temperature error matrix. This temperature error matrix was then fed into the control algorithm to create the desired control signal matrix. This control signal consisted of a matrix of optical intensities corresponding to each projection pixel (ranging from 0 – 255 on a per pixel basis). This matrix was then used to generate the control signal image sent to the projector.

4.4.3 *Normalizing the Reference Image*

For a given trial, a MATLAB script opened and normalized the reference image such that an “on” pixel had a value of 1 and an “off” pixel had a value of 0. This image was 512 pixels wide by 384 pixels tall.

4.4.4 *Error Matrix*

To generate the error matrix required to feed into the control algorithm the desired and actual temperature matrices had to be obtained. When the reference image was normalized all pixels within the sintering cross section had a value of 1 and all pixels outside of this had a value of 0. This was then multiplied by the target sintering temperature to create a matrix of target temperatures. At this point any element within the desired cross section had the value of the target temperature, and all elements outside of the desired cross section had a value of 0.

The actual temperature matrix was the result of the warping and cropping of the thermal image. MATLAB read the full frame of the thermal image and then used the values in the configuration file to appropriately warp and crop it to an image representative of the sintering area. This area was only 80 x 60 pixels, so the matrix was resized to 512 x 384 pixels to match the target temperature resolution of 512 x 384. (Note that in describing image resolution the standard is to

use *width x height* which is backwards from common matrix notation which is *rows x columns*.) The method of this resize was the MATLAB scaling function `imresize`. This is done using the default arguments which gives a bicubic interpolation [13], where the outpixel value is a weighted average of pixels in the nearest 4 x 4 grid of surrounding pixels.

With these two matrices (actual and desired temperatures) a temperature error matrix was calculated by subtracting the actual temperatures from the desired temperatures:

$$E(t) = SP(t) - PV(t) \quad (4)$$

In this equation $SP(t)$ represents the “Setpoint” matrix (target temperatures), $PV(t)$ represents the “Process Variable” matrix (actual temperatures) and $E(t)$ represents the error matrix. This temperature error matrix was now composed of the finite temperature error for each pixel, which was then passed through the control algorithm to generate the control signal (a number from 0 [no power] – 255 [100% power]).

4.4.5 Control Algorithm

The control algorithm implemented was based off of traditional feedback control, demonstrated visually in Figure 4.6.

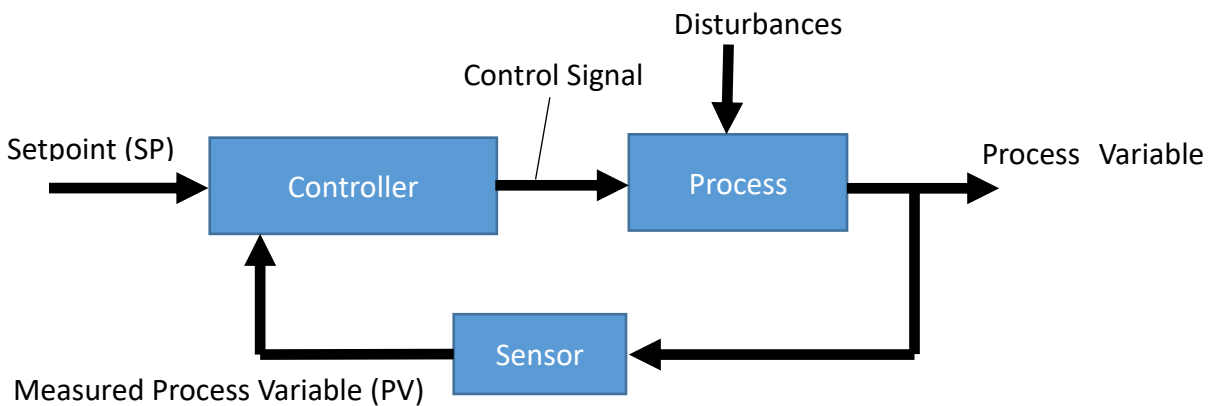


Figure 4.6 - Feedback control loop.

4.4.5.1 Proportional Control

Proportional control was implemented by multiplying the temperature error matrix by a proportional gain K_p . For example if an element was registering at 193 °C and the temperature target was 195 °C, the error would be:

$$195\text{ }^{\circ}\text{C} - 193\text{ }^{\circ}\text{C} = 2\text{ }^{\circ}\text{C}$$

Using a gain $K_p = 100$ this results in a control signal of:

$$C_s = E * K_p = 2\text{ }^{\circ}\text{C} * 100 = 200 \quad (5)$$

$$\frac{200}{255} * 100\% = 78.4\% \quad (\text{normalized}) \quad (6)$$

This represents the signal contribution from proportional control. It was recognized that proportional control is often paired with integral control to reduce steady state error and derivative control to prevent overshoot. In the limited time available within the scope of the thesis experimentation, the response from proportional control were deemed sufficient in its ability to control the heat transferred into the part. In future experiments beyond this thesis it is anticipated a more sophisticated control algorithm would be implemented.

4.4.5.2 Additional Control Signal Conditioning

This system was not capable of applying a power above 100% nor a power below 0% (it could only heat powder) so if the signal is above 255 it was considered saturated and changed to 255, while if it was below 0 it was changed to 0.

4.4.6 *Generating the Control Signal Image*

The control signal image was the one displayed to the projector, it was generated using `imwrite` in MATLAB. The `imwrite(A, 'filename.bmp')` function when given a 2-dimensional array `A`, applied a grayscale color map to the image, where a value of 0 resulted in black and then a progressively lighter gray all the way up to a value of 1 giving a white pixel. The function then wrote this image to a file. For open loop control all pixels within the desired cross section were given a value of 1 for the control signal (unless otherwise specified), representing full intensity white light. In this case the reference image and the control signal image are the same.

4.4.7 *Sending the Control Signal Image to the Projector*

The control signal image was read by a function in the Cogent third party toolbox and which displayed it on the projector by identifying the projector as a second monitor (connected via HDMI to the computer). The Cogent toolbox was a third party toolbox developed by The Laboratory of Neurobiology [14] to display images quickly to a screen to create visual stimuli. Repurposed here it proved effective at displaying full screen images on the projector (code found in the appendix). In doing this the 512 x 384 pixel image was resized to 1024 x 768 by the toolbox graphics functions. The toolbox achieved the fastest loop time when opening an image file from the current directory, rather than specifying the pixel values in a matrix and having it read these from within MATLAB as one would normally expect to be faster.

4.5 **Gray Scale Calibration**

The gray scale output is nonlinear, however at this basic level of control where net energy absorbed by the part is more important than absolute precise temperature control, it was treated as linear and the control signal was not modified to account for it, which would have slowed the loop time.

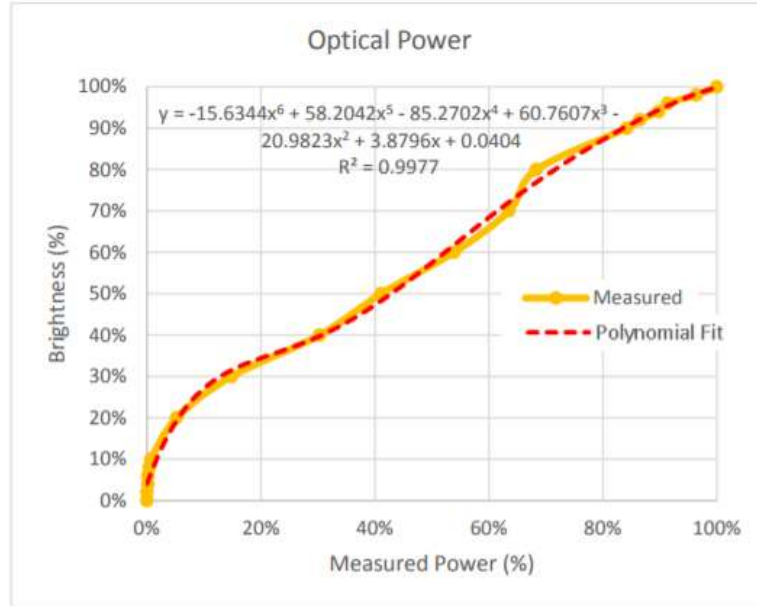


Figure 4.7 - Power calibration with gray scale (% brightness). [7]

CHAPTER 5: SYSTEM COMMISSIONING

Before proceeding to the quantitative experimentation it was important to first step through a series of trials to get a qualitative understanding of the many independent variables and their effects on the sintering process. For the experiment, the vast majority of these variables were to be held constant, but the appropriate values were unknown. The goals of these preliminary experiments were to explore the technology and settle on not only the specific independent variables that would be changed and how they would be changed in the trials, but also establish consistent operating parameters and procedures.

Near the end of these preliminary trials the projector lamp / optics were discovered to be fouled and producing significantly less optical power than what was expected. The Optoma X341 projector was replaced by a very similar Optoma X316 upon this discovery, but it's important to note that the experiments conducted in this section were done using a lower power projector (the fouled X341) with significant asymmetries in the power distribution. The Optoma X316 in its current state provided 7.7 watts of optical power, while the fouled X341 was producing 4.2 watts. This is outlined in *5.4 LAS performance stability*.

5.1 Sintering Substrate

To prevent fouling of the build plate, a glass substrate was used to fuse the first layers to in sintering. A 1/8 x 3 x 3" mirror placed on top of the build plate, this had the benefit of reflecting transmitted light back through the powder, aiding in sintering the first few layers.

5.2 Powder Bed Conduction Heating

One design objective of the powder bed was to hold the powder at as high of a temperature as possible without risking melting. With the thermistor embedded within the middle of the build plate, the heater mounted below, and a glass piece above the build plate adding thermal resistance, it was found that the temperature at the surface of the thinnest discernable layer of powder on the glass was significantly lower than the temperature of the thermistor embedded in the plate. A temperature of 176 °C was selected for the build plate. At this setting, the surface of the powder on top of the glass substrate was 165 °C for thin layers of powder. Higher set points were not considered because any powder that fell off the glass slide onto the build plate and around the gasket would have been exposed to temperatures higher than melting ($T_m = 175\text{ °C}$) and fouled the gasket / build plate. The powder started to exhibit significant clumping and some fusing to the build plate when higher temperatures were attempted.

The parts in the trials within this thesis were all less than 1 mm thick, with such thin parts small changes in the temperature of the powder bed walls had no significant effect on the temperature of the powder where the sintering took place (centrally located on the powder bed). The side heaters were still important as the main source of heat in the build chamber. The side heaters were set to 160 °C to remove any risk of powder melting, while still heating the build chamber. Because the thermistor embedded in the aluminum on the side was only covered by 1/16” of aluminum, it was assumed that the inner sidewall temperature was very close to the thermistor reading.

Using a thermocouple the temperature of the air at the top of the build chamber above the powder bed reached 100 °C in a steady state condition. From the moment the heaters were turned on this took roughly 15 minutes to achieve.

5.3 Preliminary Sintering Trials

An initial theory was that closed loop control vs open loop control would have a significant difference in measured corner radius. Of particular interest was the measurement of interior corners, so the first cross section sintered was a large square with an interior cutout. This square was 684 pixels on the exterior dimension and 300 pixels (projector pixels) on the interior dimension, which translates to 14.36 mm and 6.3 mm respectively (shown in Figure 5.1).



Figure 5.1 - A sintered interior square. On the left a) the reference image and b) the resulting sintered part. Due to non-uniformity in the projector power distribution the part showed high degrees of asymmetry, with the lower right corner not fully fusing to the layer below while the upper left corner melt pool overran its boundaries significantly.

5.3.1 Depositing Layers

The layer deposition process was characterized by moving the powder bed from the sintering area to the powder deposition area, depositing the powder at the front end of the powder bed, then moving the powder bed back to the sintering area, during which time the fixed powder scraper spreads this volume of powder smoothly over the powder bed in a new 100 μm layer.

These actions were created in a G-Code script run in Repetier for repeatability and speed, this is shown in Figure 5.2. Elevated speeds were used in traversing back and forth in the build chamber to speed up the recoating process and increase manufacturing throughput. To prevent any

jarring of the powder by acceleration forces, the jerk (rate of change of acceleration) and acceleration values were reduced in the system software, giving smooth but swift movement.

```
G91  
  
G1 Z-0.3; lower build plate 0.3 mm  
  
G1 X-155 F4000; go back (high speed - 4,000 mm/min)  
  
G1 Z0.25; raise build plate 0.25 mm  
  
G1 E4.27; deposition  
  
G1 X155 F1500; layer smoothing occurring as bed returns to sintering stage (low speed)
```

Figure 5.2 - G-code to deposit 50 micron layer. The build plate is lowered 300 microns below the scraper to ensure there is no interference, the powder bed is moved 155 mm to under the powder deposition drum, the build plate is then raised 250 microns for a net lowering of 50 microns, the drum is calibrated such that a displacement of 4.27 corresponds with two grooves of powder deposited, the powder bed is then moved back 155 mm to its original location, and as it moves the scraper spreads the deposited powder into a new layer. For 100 micron layers, the second build plate raising is reduced to 200 microns for a net lowering of 100 microns, all else is left the same.

5.3.2 Zeroing the Z-axis

In order to get this very thin first layer the powder scraper was used at a datum and zeroed. This was found by increasing the height of the build plate 10 microns at a time until mechanical interference was heard between the scraper and the glass substrate on the powder bed. Due to thermal expansion this process is done after the system is fully heated.

5.3.3 Sintering Base Layers

It was verified (after previous experiments experienced similar phenomena) that unless a very thin first layer was used and fused thoroughly to the glass substrate that the edges of the sintering cross section would curl up, ruining the next layer when it was spread.

Glass is 4x as thermally conductive as nylon in its solid state (1.05 W/m*k vs 0.25 W/m*k)[16], and the gap widens further when the nylon is in a powder state with air gaps in between particles. This meant for the first few layers it took significantly more heat to sinter the layer as the glass acted as a heat sink. Table 5-1 provides the conditions that were used to sinter the base layers with the old X341 projector and the replacement X316.

Table 5-1 Summary of base layer power exposure intensities and times.

Layer	Optoma X341 (4.2 watts) projection intensity	Optoma X316 (7.7 watts) projection intensity
First layer (50 μm)	Full power 15 seconds + medium external radiation	Full power 15 seconds + medium external radiation
Second layer (50 μm)	Full power 15 seconds + medium external radiation	Full power 12 seconds + medium external radiation
Third layer (100 μm)	Full power 10 seconds + medium external radiation	Full power 8 seconds + medium external radiation
Trial layers 4-8 (100 μm)	Trial dependent	Trial dependent

The glass heat sink effects diminished rapidly after the first few layers were deposited, with layers 4-8 were consistent in power / time to sinter. These were to be considered “trial layers”. With the top surface of the part experiencing the “trial” conditions, all measurements for cross sectional geometry were to be taken from the top surface of the finished part.

When it was discovered the X341 projector was producing low power and the X316 was put in place, these numbers were reduced for the second and third layers as summarized in Table 5-1.

5.3.4 Closed Loop Preheat

The initial method was to wait for the freshly spread powder surface to heat up to a set temperature to start a layer. This could take a substantial amount of time as the heat was conducting upward from the lower substrate. Therefore a procedure was established where as soon as the

layer was spread a 5 second closed loop preheat (using the projector) of the entire sintering area was used immediately before the sintering step. This preheat was set with a temperature target of 170, and the temperature stabilized within the preheat time to a uniform temperature distribution.

5.3.5 Sintering

In initial trials with the X341 the sintering process was more successful when external radiation was used to add radiation heat flux to the sintering area. Sintering an interior square with external radiation and full intensity open loop control a layer took 6 seconds for the melt pool to propagate satisfactorily but not propagate beyond the part boundaries significantly. Without external radiation and using full intensity open loop control, a sintering time of 10 seconds was used and there was still some edge curling.

After the X316 was put into place and more power was available, the time for a 100 micron trial layer (layers 4-8) to sinter satisfactorily dropped to 4 seconds with no external radiation. There was the option to use external radiation to speed sintering times further, but the spatial variation in power input introduced were not worth the additional power with an already faster sintering time. The external radiation was only used to sinter the base layers (1-3) in all experimental trials reported in this work.

5.3.6 Sintering Uniformity

There was notable asymmetry of the initial sintered parts. In both cases with and without external radiation, the projector melted the powder in the lower right quadrant of the projected area faster than the other areas. In open loop control as this melted first, it continued to absorb energy and the melt pool extended to areas beyond the desired cross section. This meant one corner of the interior square cross section was disproportionately larger than the rest, while on the opposite corner there was so little power that the corner was significantly blunted and not completely melted.

Switching to the X316 this problem was not nearly as prevalent, but there was still minor asymmetries in the power distribution. This is shown in *5.4.1 projector power uniformity*.

5.4 LAS Performance Stability

It was noted as experiments progressed that the powder was melting more slowly at full power despite consistent operating conditions. This was initially attributed to some visible residue building up on the glass above the sintering area, which was absorbing some of the radiation energy as it passed through the glass. The glass was lifted on one side to create an air current pulling the rising contaminants over the sintering area off to the side to avoid hitting the glass right where the light passed through, also any accumulated residue was wiped away in between builds to keep it at a minimum.

It is characteristic of projector lamps to get significantly dimmer in the early stages of their lives, and then a slow degradation after that, where at the end of the lamp's useful life it is only about 50% as bright, with the life of the lamp advertised as 5,000 hours for the X341 and X316 at a full brightness setting [12]. As a check, the power of the projector (with 40 hours of use) was measured just beyond the final lens at 4.2 watts. In comparison the X316, with a slightly lower lumen specification (3200 vs 3300 lumens) was measured to have 7.2 watts with 80 hours of use. The lamps from the projectors were switched and the experiments repeated, with the power from the X316 lamp resulting in 3.7 watts. This gave the clear result that the lamp on the projector was not the issue, with the same lamp producing 7.2 watts in one projector and 3.7 in the other. The most logical explanation was that the optics of the X341 in use on the system were fouled. This was the basis for replacing the X341 projector with an X316 that was available.

5.4.1 Projector Power Uniformity

In trials with the original projector it was very clear that there was substantially more power being applied to the top left corner of the projector reference frame with a smaller amount available to the lower right hand corner. This non-uniformity was not quantified as the original projector was clearly not usable without substantial investigation / cleaning that may not have been possible, but an experiment was done to characterize the power uniformity of the X316.

In order to do this, the projection area was divided into a 4 x 3 grid and only one grid element at a time was turned on to full power (100% white light). A THORLABS PM100USB power and energy meter (signal conditioner), model number S310C, was used to measure the radiation energy for each element. This was a manual process, done by making very small adjustments to the orientation of the power meter to converge to a maximum power value.

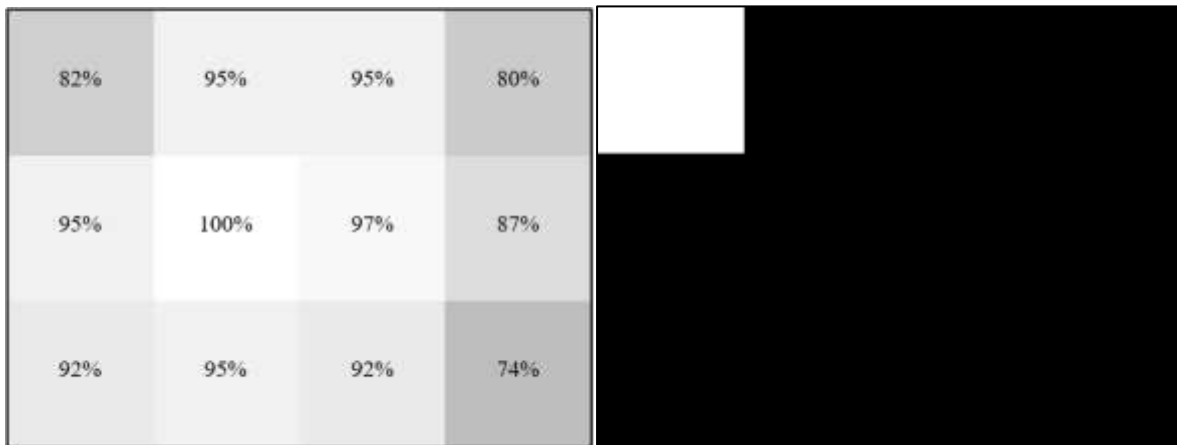


Figure 5.3 - The power uniformity of the projector. A low resolution power distribution of the projector normalized to the most powerful element (left). An example of the image sent to the projector to measure the power for the uppermost left element – the “white” area is exactly 1/4 of the image width and 1/3 of the image height (right).

These power measurements were slightly offset by the fact that the black area surrounding the white square was not truly void of radiation when the image was projected. There was some light still transmitted, and for a full black screen it was measured that there was 27 milliwatts of

power being emitted. Taking into account the “on” pixel this would mean that there was an average of 24.75 milliwatts of black area energy added to every power measurement. The total sum of all of the elements was 8.0 watts, but keeping in mind that the black area energy had to be subtracted from every measurement to get just the contribution of the white light, the total power reduced to 7.7 watts which was considered to be the full power capability of the projector. The 7.2 watts earlier measured was taken on a full frame white image from the projector which was challenging to converge to an absolute highest power.

In terms of performance of the system, more power allows for faster rise times which increases the ability to control the thermal history of the part. In addition, this can lead to layers that are sintered more quickly, increasing manufacturing throughput. A final benefit of this is that there is less time for thermal gradients to occur in the X-Y plane, reducing risk of melt pool propagation beyond the cross section boundaries.

5.5 Trial Procedure

With the goal of repeatable experimentation, a consistent trial procedure was selected based on observations in the preliminary experimentation. The standard trial procedure for all builds was as follows:

- 1) Control box turned on, this turns on all projector fans and provides power for the heater relays and RAMPS 1.4 module which powers the stepper motors.
- 2) In Repetier, the build plate is set to 176 °C with the walls set to 160 °C, system left for 15 minutes to heat (On physical control computer).
- 3) In Repetier, X and Z-axes zeroed.
- 4) In Repetier, powder bed moved to 170 mm on the X-axis.
- 5) Projector powered on.
- 6) Sintering_startup MATLAB script run (on sintering computer) [script in appendix B]

- 7) Layer deposition script in Repetier (shown in figure 5.2) used to deposit 50 micron layer.
- 8) First 50 micron layer sintered 100% power for 15 seconds, low power external radiation.
- 9) Repetier script used to deposit second 50 micron layer.
- 10) Second 50 micron layer sintered 100% power for 12 seconds, low power external radiation.
- 11) Repetier script used to deposit 100 micron layer (3rd layer).
- 12) Third layer sintered 100% power for 8 seconds with low power external radiation.
- 13) Sintering_startup MATLAB script automatically closes.
- 14) Trial layers (layers 4 – 8).
- 15) Sintering_trials MATLAB script run [script in appendix B]
 - a. Repetier Script used to deposit 100 micron layer
 - b. 5 second layer preheat step (closed loop, 170°C target)
 - c. 4 second sintering step (closed loop or open loop depending on trial)
 - d. Repeat steps b – d until the 8th layer is sintered
 - e. Sintering_trials MATLAB script automatically closes

CHAPTER 6: EXPERIMENTATION

6.1 Experimental Goals

The most significant independent variable introduced in moving from the first generation system to this system was the integrated infrared camera, coupled with the additional software to geometrically associate the temperature data accurately to the sintering cross section. This allowed the ability to implement point-wise closed loop temperature control of the sintering cross section, and beyond this, allowed the logging of temperature data as a function of position in the sintering cross section for each part built. This temperature data could then be referenced after the fact for both open and closed loop trials to further understand the final part properties observed.

A high priority was to observe any feature resolution improvements due to the implementation of closed loop control, to see if the idea warranted further investigation. It was demonstrated in *2.1.2 heating a square of powder* that the interior area of a sintering cross section in open loop control heats at a much higher rate than the surrounding edges. In order to sinter the edges fully, longer sintering times are used and the central areas are heated well beyond the necessary amount, leaving a high temperature melt pool with the opportunity to overrun interior features. Melt pool overrun is characterized by propagation of the melt pool beyond the cross section boundaries. The cross section chosen to test was one where a feature was exposed to these excess temperatures in the bulk area of the sintering cross section, to give the best chance of a notable difference between open and closed loop control.

6.2 Cross Section Tested

6.2.1 Making the Cross Section Reference Images

For each sintered part, a 512 x 384 pixel cross section reference image was required. It was found that the best tool to create cross section reference images was Power Point. This allowed the user to create shapes of specific sizes and specify their location on the image precisely using length parameters built into the software.

6.2.2 High Aspect Ratio Notches

The cross section settled on was a square with a high aspect ratio notch in each side, protruding into the sintering area. These thin lines of unheated powder would be susceptible to melt pool overrun from the center and sides.



Figure 6.1 - HAR interior notch reference images (left - 40 x 60; right 40 x 160 pixels).

It was best to use nominal pixel sizes to define the notches as there is no way for the projector to “split” a pixel, while measurement tools could easily resolve the distances in the sintered part later. The squares had 600 pixel (1.26 cm) edge dimensions and the centrally located notches ranged from 40x60 to 40x160 pixels (0.84x1.26 to 0.84x3.36 mm).

6.3 Experimental Trials

6.3.1 Independent Variables Tested

The experiment compared open vs. point-wise closed loop control. The open loop trial cross sections all received 100% power for 4 seconds. The closed loop control was given a temperature target of 195 °C and used a proportional gain k_p of 30 to determine the radiation intensity profile as a function of temperature, also for 4 seconds.

6.3.2 List of Experiments

This section outlines the experimental trials done and the associated independent and dependent variables considered, shown in Table 6-1.

Table 6-1 Summary of experimental trial parameters. The only difference between closed and open loop trials was the sintering intensity.

Interior High Aspect Ratio Notch - Open Loop Control		
Relevant independent variables		Dependent variables measured
Sintering time	4 seconds (constant)	- Draft angle
Sintering intensity	100% power (Open loop)	- Width at top of notch (microns)
	Dynamic power (Closed loop)	
Nominal notch width	40 pixels (833 microns)	- Width at bottom of notch (microns)
Nominal notch depth	60 pixels (1.25 mm)	- Corner radii (microns)
	80 pixels (1.66 mm)	- Notch depth (mm)
	100 pixels (2.08 mm)	
	120 pixels (2.50 mm)	
	140 pixels (2.92 mm)	
	160 pixels (3.33 mm)	

6.4 Results

6.4.1 Thermal Data

MATLAB structures were used to log the geometrically adjusted and cropped temperature data from the sintering cross section and store it for each loop iteration. An example of the spatial temperature distribution during the trials is shown in Figure 6.2.

6.4.1.1 Thermal Cross Sections

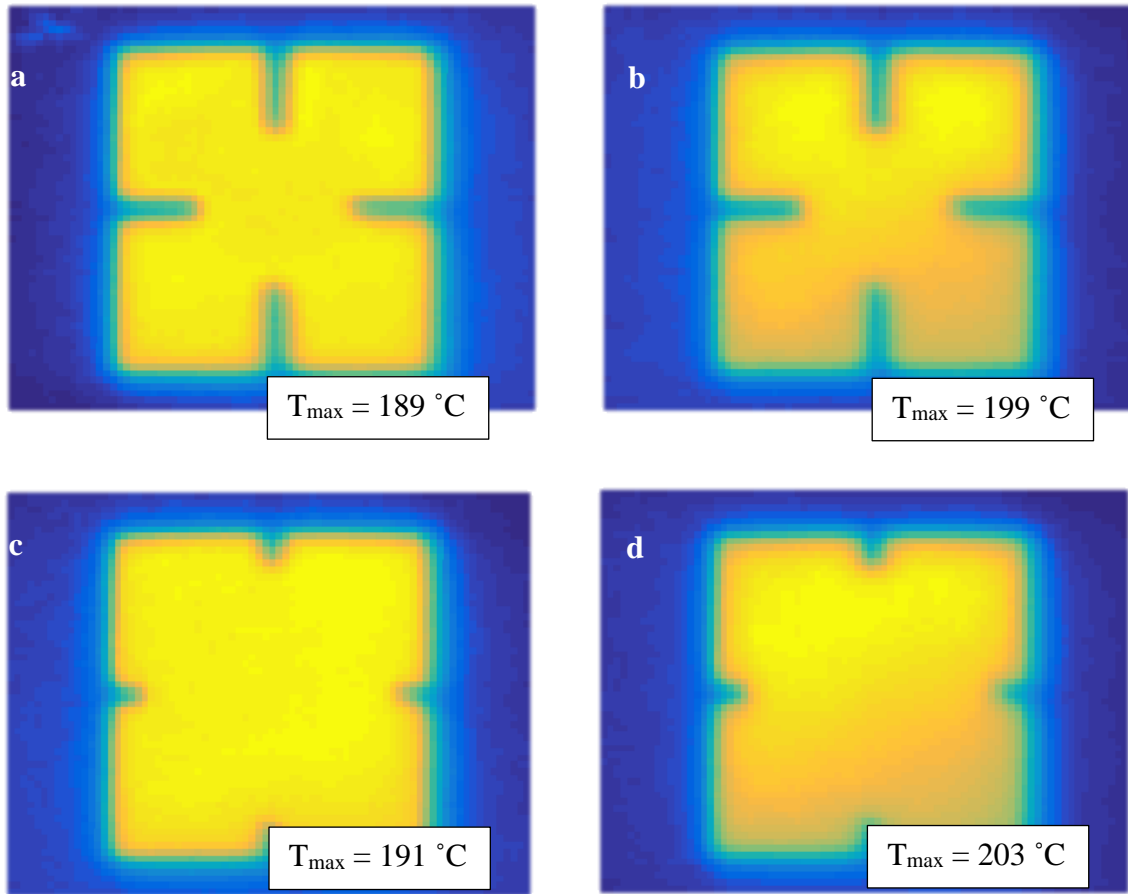


Figure 6.2 - HAR notch thermal images at 3.5 seconds into sintering. a) 40 x 160 Closed loop b) 40 x 160 Open loop c) 40 x 60 Closed loop d) 40 x 60 Open loop. Note the non-uniformity of heating in the open loop case. The image scales are normalized, so it appears that the maximum temperatures are the same between the cases, but the open loop trial maximum temperature is substantially higher.

6.4.1.2 Thermal Data Graphs

To validate the implementation of point wise temperature control, thermal data was recorded for the sintering cross sections as a function of time and position. The temperature at the middle of the cross section was pulled out of this data as well as the temperature at the corner as a reference for the slowest heating area of the part. A “slice” of temperature data was taken across the sintering cross section horizontally straight through the notches. This highlights the

temperature gradients occurring in the process as well as the ability to view the effects of closed loop control.

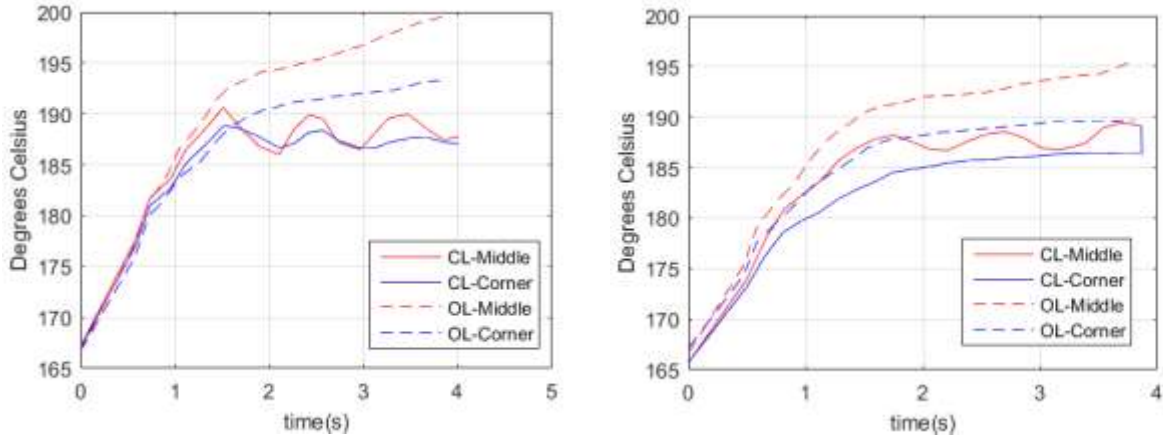


Figure 6.3 – Temperature response at the middle and corner of the sintering cross section. This is for a 40 x 60 (left) and 40 x 160 (right) interior notch specimen

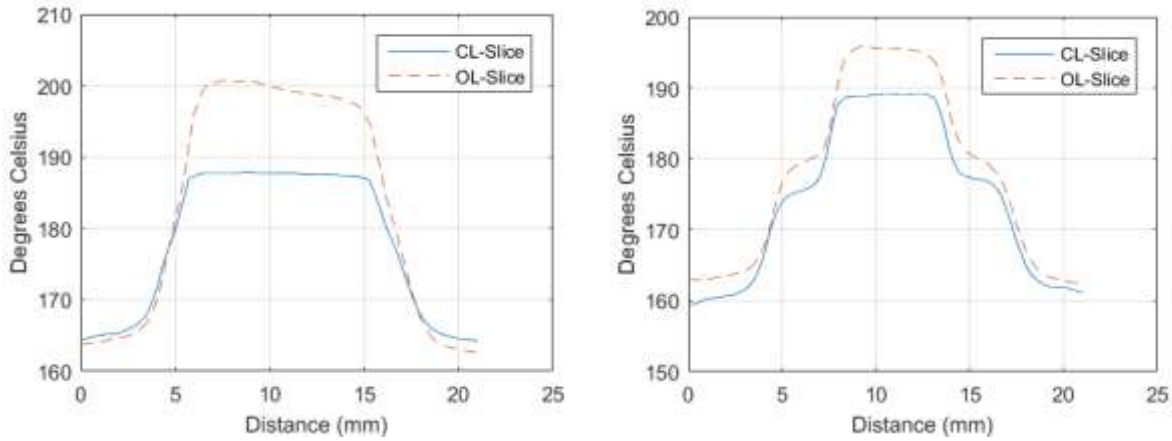


Figure 6.4 – Temperature data along a line through the cross section. This is for a 40 x 60 (left) and 40 x 160 (right) interior notch specimen

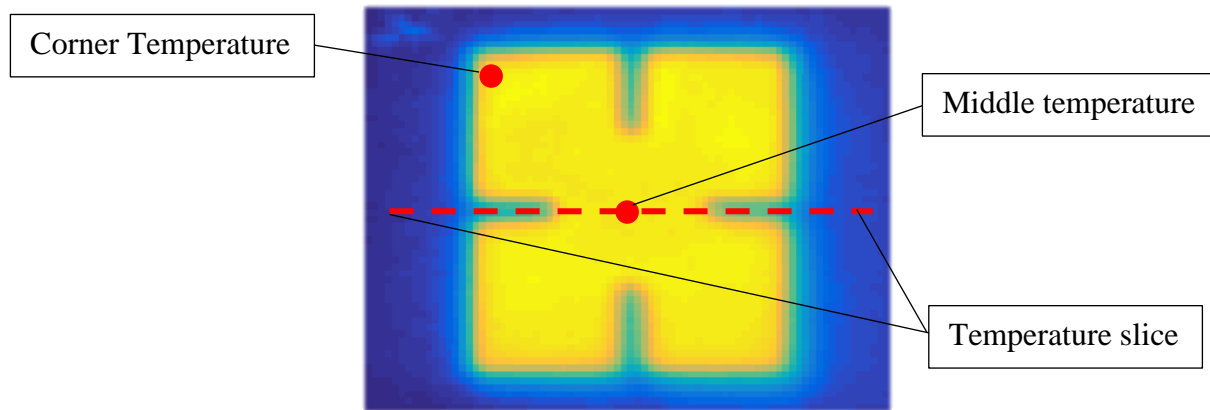


Figure 6.5 - Visual representation of where the data was taken for figures 6.3-4.

6.4.2 Geometrical Data

In addition to controlling and monitoring the thermal history of the sintering parts, the resulting geometry was analyzed and compared to the nominal dimensions of the target cross section. The goal here was to both characterize the results of open loop control and find correlations between improved feature resolution and point wise closed loop temperature control.

6.4.2.1 Measurement Procedure

The cross section geometry was observed using a Dino-Lite USB microscope camera and the accompanying software DinoCapture 2.0. In the finished sintered parts, each of the four notches on each specimen were analyzed to measure the upper corner radius, the draft angle (angle between the two sides of the notch), the width of the notch at the bottom, the width of the notch at the top, and the overall notch depth. The temperature matrices for the sintering cross sections throughout the build were also tracked. The geometrical measurements captured are summarized in the figure on the next page.

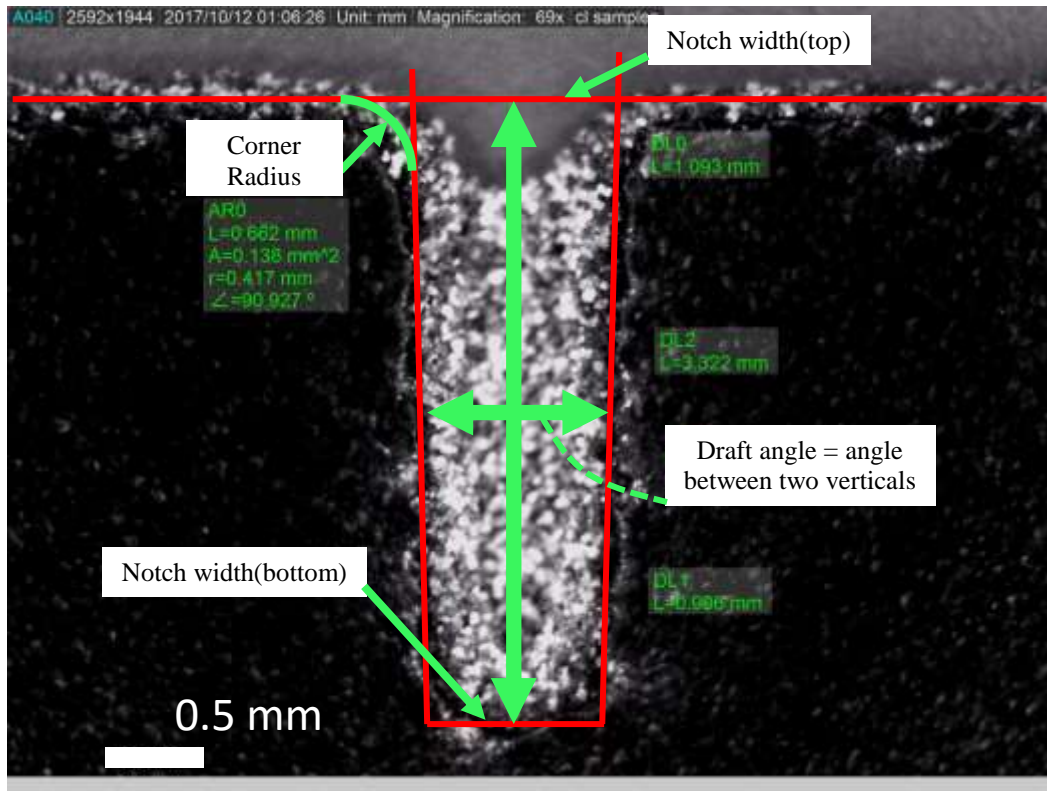


Figure 6.6 - Optical measurement of notch geometry. The dependent variables measured are identified by the following in the figure: ARO - corner radius, DLO - width at top, DL1 - width at bottom, DL2 - depth, FA0 - draft angle.

6.4.2.2 Images

The images below are representative of the parts sintered in the trials, with all of them finishing very similar to this.

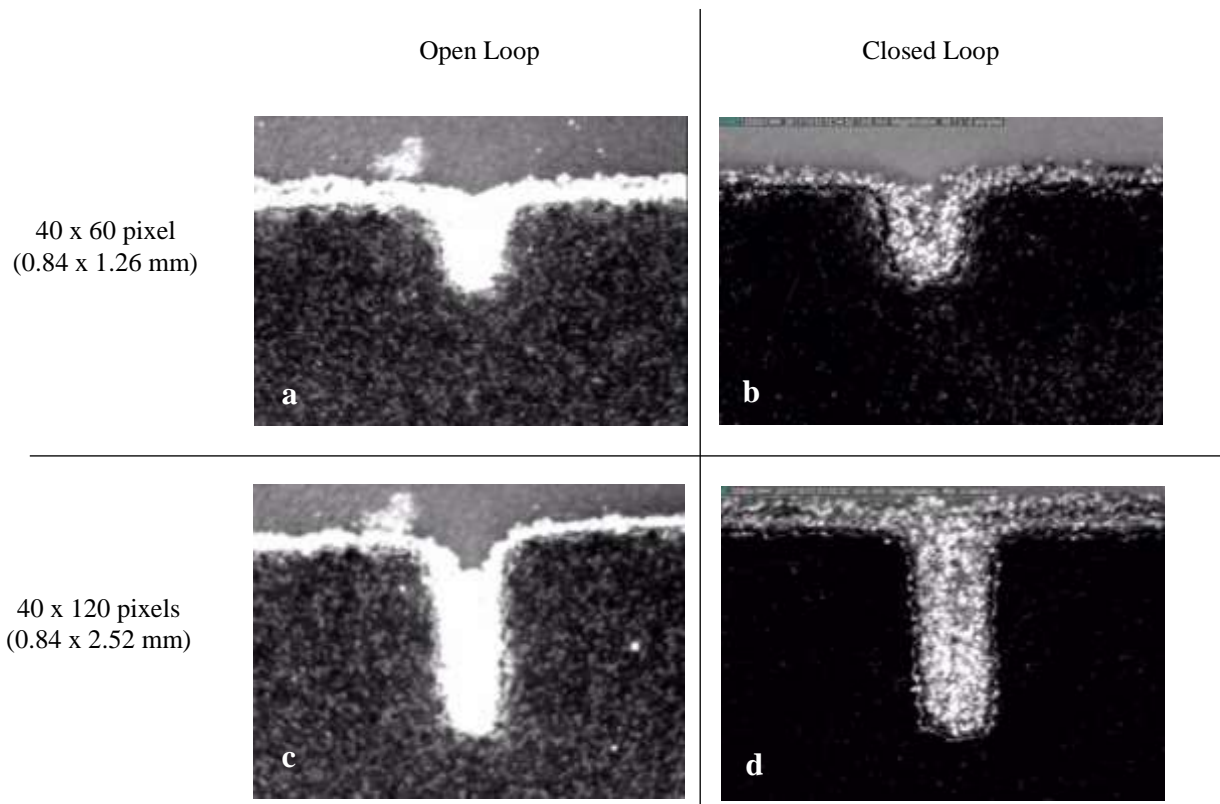


Figure 6.7 - High aspect ratio notch specimen images. a) 40 x 60 pixel open loop control b) 40 x 60 pixel closed loop control.c) 40 x 120 pixel open loop control and d) 40 x 120 pixel closed loop control. Note the increased draft angle of the open loop control parts, and the closed loop control parts characterized by having a cleaner, more rectangular profile. Magnification is 70x.

6.4.2.3 Graphs

For each experimental trial there were 4 data points taken (each of the 4 notches on one part), and the averages of these values are reported here.

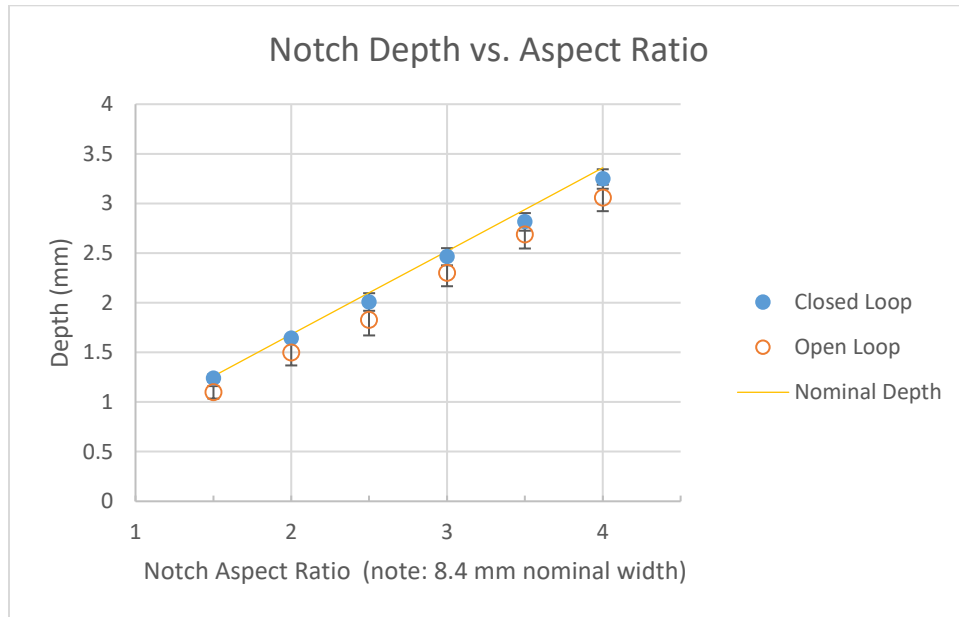


Figure 6.8 - Notch depth vs Aspect ratio. This graph shows a consistent trend of the closed loop control performing more accurately than the open loop control.

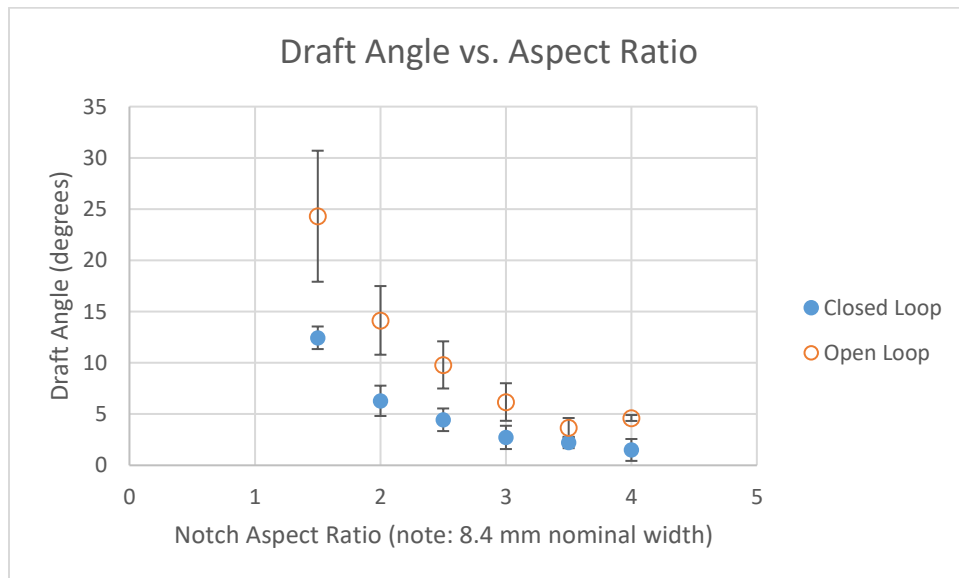


Figure 6.9 - Draft angle vs. Aspect ratio. This again shows a correlation of improved geometry with closed loop control

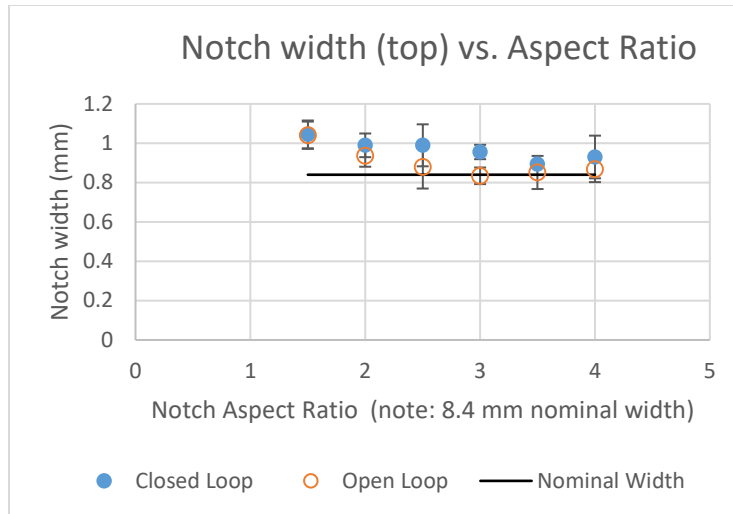


Figure 6.10 - Notch width (top) vs Aspect ratio. The width at the top was consistently wider than the width at the bottom of the notches. This is likely due to the fact that at the top are two exterior corners, which have large amounts of unheated powder around them, while the corners at the bottom are interior corners, surrounded by much more heat, sintering more readily. This metric was worse with closed loop control, but it is likely that open loop's better performance was a side-effect of the overrun of the melt pool into the notch, and not a positive benefit of open loop control.

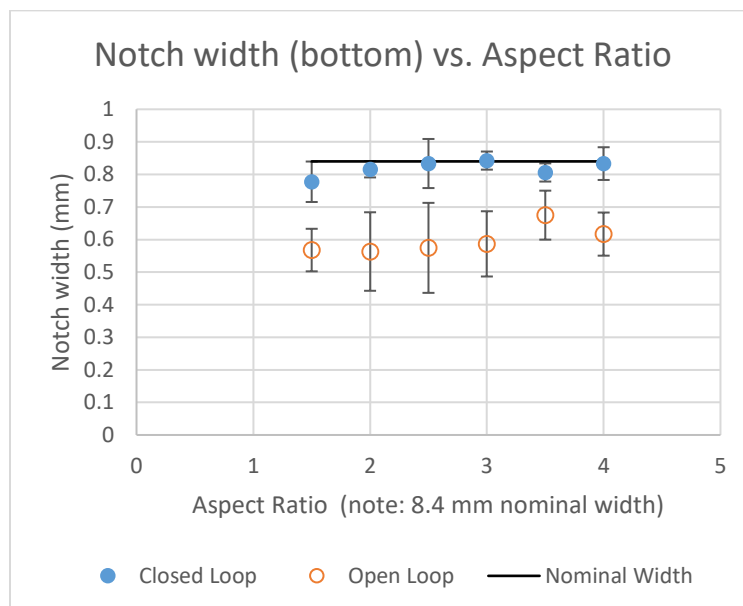


Figure 6.11 - Notch width (bottom) vs. Aspect ratio. This was significantly impacted by the addition of closed loop control. Likely because the bottom of the notches are closer to the central areas of the part which can overheat in open loop control.

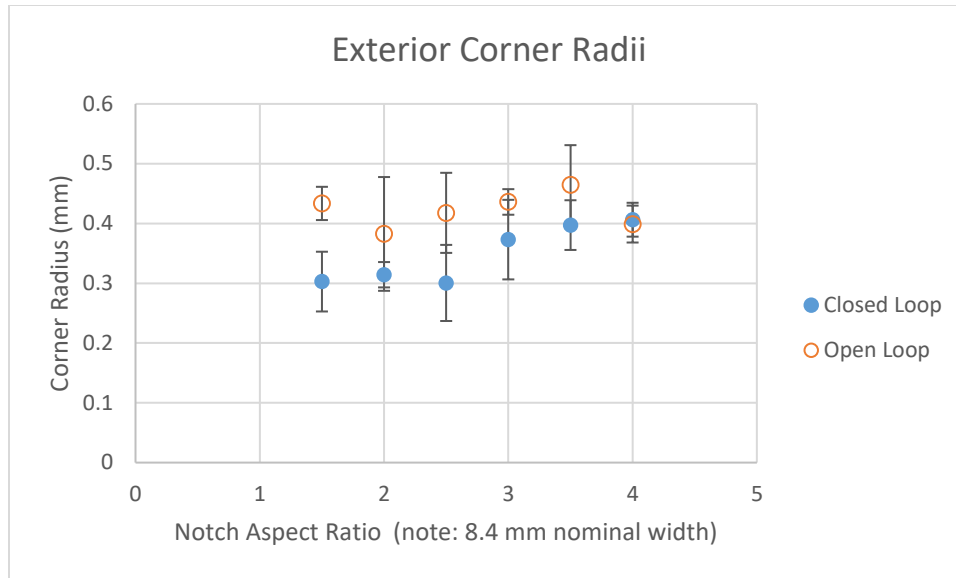


Figure 6.12 Exterior corner radius vs Aspect ratio. The radii were in general sharper with closed loop control.

6.4.2.4 Statistics on Significant Findings

It was noted that there were significant improvements especially to the notch depth accuracy and the notch width at the bottom, both areas that were in close proximity to the higher temperature middle of the part. Table 6-2 quantifies these benefits with statistics.

Table 6-2 Summary of notable statistics. Notch depth and the notch width at the bottom were the variables that saw the most significant improvement between open loop and closed loop control. The errors between the actual values and the nominal values are summarized here.

	Notch depth error (distance short of nominal depth)		Notch width (bottom) error (distance short of nominal width)	
	Open Loop Control	Closed Loop Control	Open Loop Control	Closed Loop Control
Mean	233 μm	74 μm	243 μm	22 μm
Std. Dev.	121 μm	77 μm	94 μm	48 μm

6.5 Discussion

The purpose of this experimentation was to validate the functionality of the system as a large area sintering test platform, to verify the ability to implement point wise temperature control, and as a secondary goal find compelling reason for further experimentation on the use of closed loop control to improve feature resolution.

The thermal data shown in section 6.4.1 Thermal Data give clear evidence that the point wise temperature control, even with its very simple control algorithm, was capable of restricting the maximum temperature rise within the sintering cross section, and holding the temperature to a bounded output. With a more sophisticated control algorithm and the much faster loop time afforded by purpose built software / hardware in an industrial setting, the response would be further improved.

The temperature data gives meaningful insight into the geometrical results measured. In the following sections the data will be used qualitatively along with general knowledge of the sintering process outlined in Ch. 2 to help explain these results.

6.5.1 Notch Depths

The depth of the high aspect ratio interior notches experienced exceptional improvements with the addition of closed loop control. In both the open and closed loop cases (see Figure 6.7), the notches were shallower than their nominal dimension due to melt pool overrun, but closed loop control improved the performance dramatically. The average closed loop depth error was 74 μm over 24 samples (6 specimens each with 4 notches), with a standard deviation of 77 μm . The average open loop depth error was 233 μm , with a standard deviation of 121 μm over the same sample size.

The central reason why the high aspect ratio notches were chosen was because they reached further into the central area of the part, where temperatures are documented to be higher. Figure 6.4 clearly shows how the closed loop control halts this temperature rise in the central area of the part, reducing the excess energy absorbed by the cross section that would then turn into an overrun melt pool.

6.5.2 *Notch Widths*

The discrepancy in the width of the notches can be largely explained by the difference in melt pool overrun as a function of notch depth. The melt pool starts in the center and moves outwards, which means that the areas deeper within the notch are exposed to hot and viscous molten polymer for a longer period of time than the edges. Also there is minimal unheated powder in the depth of the notch compared to at the notch opening. The extra cooling available closer to the edge inhibits the propagation of the melt pool. These two factors together contribute to the notches being narrower at the bottom than at the opening (see Figures 6.9, 10). Closed loop control improved the notch bottom width metric by limiting the temperature gradients in the X-Y plane, along with reducing the excess energy placed into the viscous melt pool that would enable it to propagate further into unheated powder. The top width proved to perform slightly worse in closed loop control, but this is likely a correlation with melt pool overrun making a negative feature thinner rather than a correlation with better accuracy with open loop control.

6.5.3 *Notch Draft Angle*

This is coupled with the notch depth and width metrics. A notch with a wider top width and a narrower bottom width will have a larger draft angle, as will a shallower notch resulting from an overrun melt pool. Closed loop temperature control inhibits these effects resulting in less feature distortion (verified in data shown in Figure 6.8).

6.5.4 *Notch Exterior Corner Radii*

The corner radii phenomena observed is more challenging to understand, warranting further experiments. One possible explanation is that in open loop control, the adjacent sides to the exterior corner experience more melt pool overrun as distance from the corner increases (due to the corner cooling). This would have the effect of blunting the corner. These results are shown in Figure 6.11.

6.5.5 *General Discussion*

When the melt pool is heated with more energy than necessary to sinter the layer, the excess energy is transferred to the surroundings as it is heating and then as it cools. In conduction heat transfer within the powder bed, this occurs in the form of temperature gradients even after the radiation is stopped. As the residual energy travels outwards and downwards, some of this is absorbed by the heat of fusion of adjacent powder particles that fall outside of the desired sintering cross section, as they melt. This melt pool overrun is a central cause for most of the errors observed in the part geometries, and in visual observation was seen to continue to propagate after the projector turned off.

The addition of point wise closed loop control allows the opportunity to limit the amount of additional energy put into the sintering cross sections, limiting the related melt pool overrun. This, in addition to the ability to hold the sintering process within a bounded temperature window allowing new process materials, leaves compelling reason for further investigation of point wise temperature control in large area sintering.

CHAPTER 7: CONCLUSION

7.1 Evaluation of Thesis Statement

The focus of this study was the design, construction, and validation of a large area sintering test platform. This test platform was to enable further exploration of the hypothesis that longer and controlled heating rates in Large Area Sintering would allow the capability to process a wider range of materials, as well as allow more control over the resulting final part properties.

In order to control these heating rates, the system implemented point-wise closed-loop temperature control using an integrated infrared camera. This point-wise temperature control proved effective in improving geometric accuracy as can be seen in figures 6.2 - 4 in the results section of this thesis. In these figures, open loop control is shown to result in asymmetric and excessive heating in the central areas of the sintering cross section, while the closed loop control resulted in a bounded, more uniform temperature response.

It was also demonstrated that there is a basis for the hypothesis that point wise closed loop temperature control can result in better cross section feature resolution, a key criteria for commercialization of an additive manufacturing technology. Further exploration of this is warranted.

By implementing repeatable processes for layer spreading and creating consistent powder bed preheat conditions, the system serves as an effective platform for further large area sintering experiments to be conducted. The integrated thermal camera also allows for validation of

processed parts, by providing detailed temperature data to ensure the distribution stayed within a defined process temperature window.

7.2 Comments and Future Work Recommendations

7.2.1 Future Experiments

An investigation into the melt pool propagation in the X-Y plane and Z-direction as layers are sintered and fused together would be of great use. Capillary action could be considered as well as the effects of the viscosity of the melted polymer. It would be very valuable to understand the energy density requirements and other parameters involved in getting the highest mechanical properties from a given material. A resolution study would be incomplete without taking into consideration the effects that the changed parameters have on the other final properties of the part.

The system in its current control algorithm considered a target sintering temperature but did not control the heating rate control specifically. This capability now exists, and novel experiments could be done exploring these effects. Further experiments are also warranted in using narrow temperature window process materials, as well as introducing a greater variation in process parameters with currently used materials to further understand the resulting mechanical properties. This includes but is not limited to sintering the cross section with active fill patterns, where the radiation pattern changes as a function of time to propagate the melt pool in predictable and desirable ways.

Regarding a study on the implementation of point wise temperature control to improve feature resolution, a deeper look is warranted to distinguish whether the thermal camera resolution on the print bed (~400 μm pixel size) is a limiting factor with this system. At this size the system is serving mostly to control bulk temperatures which can somewhat affect the propagation of the melt pool, but future investigation would look into whether, at the current power / projector

resolution levels, sharp enough temperature gradients can be created, where higher resolution closed loop control would be of value.

7.2.2 *Future System Improvements*

The ability to control heating rates with a very simple control algorithm was demonstrated but there is significant room for improvement both in the control algorithm used and system hardware. Another limitation of the system is peak radiation heat flux it can supply. The system used a 190 watt projector lamp giving 7.2 watts of optical power at the lens, over a sintering area of 3 cm²; to scale this up to a 10 x 10 cm area – still relatively small by industry standards – it would take a 6.3 kW projector lamp assuming the same efficiencies. At this point, the DLP chip in the projector (digital micromirror device that turns the individual pixels on and off) is a limiting factor as it can only take so much heat, and the price goes up quickly. A breakthrough for LAS would be an advancement in the way radiation energy can be patterned and controlled beyond the conventional DLP projector technology currently used.

REFERENCES

- [1] T. T. Wohlers, Wohler's Report: 3D Printing and Additive Manufacturing State of the Industry. Fort Collins: Wohlers Associates, 2015.
- [2] I. Gibson, D. W. Rosen, and B. Stucker, Additive Manufacturing Technologies: Rapid Prototyping to Direct Digital Manufacturing. New York: Springer, 2010.
- [3] R. D. Goodridge, C. J. Tuck, and R. J. M. Hague, "Laser sintering of polyamides and other polymers," Progress in Materials Science, vol. 57, pp. 229-67, 02/ 2012.
- [4] D. M. J. Williams, C. Deckard, "Selective Laser Sintering Part Strength as a Function of Andrew Number, Scan Rate and Spot Size," in Solid Free Form Fabrication Symposium, Austin, Texas, 1996.
- [5] from justin's paper, P. Peyre, Y. Rouchause, D. Defauchy, and G. Régnier, "Experimental and numerical analysis of the selective laser sintering (SLS) of PA12 and PEKK semi-crystalline polymers," Journal of Materials Processing Tech., vol. 225, pp. 326-336, 11/1/November 2015 2015.
- [6] Guaras, M. P., Alvarez, V. A., & Luduena, L. N. (2015). Processing and characterization of thermoplastic starch/polycaprolactone/compatibilizer ternary blends for packaging applications. Journal Of Polymer Research, (9), 1. doi:10.1007/s10965-015-0817-0
- [7] J. Nussbaum, N. Crane, "Evaluation of processing variables in large area polymer sintering of single layer components, " in Solid Free Form Fabrication Symposium, Austin, Texas, 2017.
- [8] Shane Collins. Standard Guide for Determining Global Energy Density of Metal Laser Sintering Systems. In order to compare metal laser sintering systems and materials a standardized method of determining the global energy density needs to be established. (6-10-2015).
- [9] A. Greco and A. Maffezzoli, "Polymer melting and polymer powder sintering by thermal analysis," Journal of Thermal Analysis & Calorimetry, vol. 72, pp. 1167-1174, 2003.
- [10] M. Vasquez, B. Haworth, and N. Hopkinson, "Methods for quantifying the stable sintering region in laser sintered polyamide-12," Polymer Engineering and Science, p. 1230, 2013.

- [11] “Optoma 341 DLP XGA Business Projector.” <https://www.optomausa.com/projectorproduct/x341>. Optoma USA, Web. 9 Sep. 2017.
- [12] “Optoma 316 DLP XGA Business Projector.” <https://www.optomausa.com/projectorproduct/x316>. Optoma USA, Web. 9 Sep. 2017.
- [13] “Resize Image – MATLAB imresize.” <https://www.mathworks.com/help/images/ref/imresize.html>. MathWorks, Web. 15 Oct. 2017.
- [14] “Cogent || Wellcome Laboratory of Nuerobiology.” <http://www.vislab.ucl.ac.uk/cogent.php>. Laboratory of Nuerobiology, Web. 10 Jul. 2017.
- [15] “Thermal Conductivity of Common Materials and Gases.” https://www.engineeringtoolbox.com/thermal-conductivity-d_429.html. Engineering Toolbox, Web. 15 Oct. 2017.

APPENDIX A: PURCHASING LOCATION OF IMPORTANT COMPONENTS

Component	Use	Purchasing info
1/8" Fiberglass rope	Gasket for sealing build plate in powder bed	McMaster-Carr (P/N 8818K42)
High-Temperature Rigid Fiberglass Insulation	Insulation for build chamber	McMaster-Carr (P/N 9350K1)
3x3", 120V A/C, 90 Watt strip heater	heating powder bed, 4 sides and build plate	Grainger Industrial Supply (Item # 6TFJ5)
High temperature silicone adhesive	Adhesive for gasket and heaters	Grainger Industrial Supply (Item # 1FBH9)
100-240 V A/C Solid state relays	To turn on heaters	Amazon
Ramps 1.4 Controller Shield	To control heaters and stepper motors	Amazon
Arduino Mega 2560	Base for ramps 1.4 controller board	Amazon
60W narrow beam (10°) halogen	External Radiation	Batteries + Bulbs - UltraLast PAR16 120V60W 10
Drivetrain and chassis components	Drivetrain and chassis components	www.openbuildspartstore.com
Open Builds	Tee nuts	SKU 536
Open Builds	Metal V Wheel Kit	SKU 505
Open Builds	Delrin V Wheel Kit	SKU 500
Open Builds	OpenRail Gantry Plate	SKU 2060
Open Builds	V - Slot Linear Rail	SKU 215 - LP
Open Builds	Eccentric Spacer	SKU 226
Open Builds	Cast Corner Bracket	SKU 490
Open Builds	Low Profile Screws M5	SKU 878
Open Builds	V-Slot Linear Actuator Bundle (belt driven)	SKU 1076
Open Builds	Cube Corner Connector	SKU 941
Open Builds	Black Angle Corner Connector	SKU 540
Open Builds	T Joining Plate	SKU 615
Open Builds	Motor Mount Plate - NEMA 17	SKU 575
Open Builds	NEMA 17 Stepper Motor	SKU 623
Open Builds	Smooth Idler Pulley Wheel Kit	SKU 550
Open Builds	GT2 - Timing Pulley - 20 tooth	SKU 210
Open Builds	GT2-2M Timing Belt	SKU 470

APPENDIX B: CRITICAL MATLAB SCRIPTS

Configuration script:

% example of config file:

% focus_constant

% 200

% t_matrix

% 7.0000 7.0000 7.0000

% 6.0000 6.0000 6.0000

% 1.0000 1.0000 1.0000

% kp ki kd

% 2 0 0

% Sintering Time

% 5

% Max Temperature

% 185

%% calibration step

clear variables

close all

clc

%% Camera Setup

% Clears the Camera in Case We Stop Mid-Print

delete(imaqfind)

```

% Object Naming and Parameters

vid = videoinput('gige');
source = vid.Source;
source.IRFormat = 'TemperatureLinear10mK';

vid.TriggerRepeat = Inf;
vid.FramesPerTrigger = 1;
vid.FrameGrabInterval = 1;
flushdata(vid);

% Change Value to Change Focus
src.FocusPos = 800;

%% Figures Setup

%% Calibration

% Calibration Used for Warp/Transformations
% [c1,r1,P1] = the 4 corners of the original square image

% c1 = [1;320;320;1]; %Results of the impixel. Aka the 4 corners x-value ; projector reference frame?
% r1 = [240;240;1;1]; %Results of the impixel. Aka the 4 corners y-value
% note: should this be 1024 x 768?
% note: image transform will map PID to this resolution

% c1 = [1;1024;1024;1]; % 4 corners x-value ; projector reference frame?
% r1 = [768;768;1;1]; % 4 corners y-value

c1 = [1;80;80;1]; % 4 corners x-value ; projector reference frame?
r1 = [60;60;1;1]; % 4 corners y-value

% Start streaming data

```



```

start(vid);
% Wait for a frame to be available before entering loop
tic
while (vid.FramesAvailable <1)
    pause(0.01);
end
radius = 30;
toc
cgloadlib
    cgopen(3,0,0,2)
    cgpencol(1,1,1)
    x = -512;
    for(i = 1:radius) % top left
        y = 384;
        for(j = 1:radius)
            cgdraw(x,y)
            y = y-1;
        end
        x = x+1;
    end
    x = 511;
    for(i = 1:radius) % top right
        y = 384;
        for(j = 1:radius)
            cgdraw(x,y)
            y = y-1;
        end
        x = x-1;
    end
end

x = -512;

```

```

for(i = 1:30) % btm left
    y = -383;
    for(j = 1:radius)
        cgdraw(x,y)
        y = y+1;
    end
    x = x+1;
end

x = 511;
for(i = 1:radius) % btm right
    y = -383;
    for(j = 1:radius)
        cgdraw(x,y)
        y = y+1;
    end
    x = x-1;
end
cgflip
pause(5)

tic
% Clearing Memory for Next Loop
    flushdata(vid); %Flushes Memory it Doesn't Reach Limit

    while (vid.FramesAvailable <1)
        pause(0.05);
    end
croptemp = double(getdata(vid)); % get data from video object
toc
stop(vid);

flushdata(vid);

```

```

cgshut
% figure(hFig)
% imshow(blank)
croptemp = (croptemp * 0.01)-273.15; % convert to celsius?

%croptemp = double(imresize(croptemp,[1024 768])); % interpolates to a higher resolution

fig5 = figure('Name','Calibration Figure','color','k'); %displays in the middle of the main screen?

% top right - bottom right - bottom left - top left
image(croptemp,'CDataMapping','scaled') % this is the full thermal camera image
[c2,r2,P2] = impixel(); % corners of calibration box in thermal camera ref frame

%% get max temp pixels
    hold on

    pixel_dist = 10;
    n = 1;
    %top right
    temp1 = croptemp((r2(n)-pixel_dist):(r2(n)+pixel_dist),(c2(n)-pixel_dist):(c2(n)+pixel_dist),1);
    [max_num,max_idx] = max(temp1(:));
    [y,x]=ind2sub(size(temp1),max_idx);
    c2(n) = c2(n)-pixel_dist + x - 1+1;
    r2(n) = r2(n) - pixel_dist + y - 1-1;

    n = 2;
    %bottom right
    temp2 = croptemp((r2(n)-pixel_dist):(r2(n)+pixel_dist),(c2(n)-pixel_dist):(c2(n)+pixel_dist),1);
    [max_num,max_idx] = max(temp2(:));
    [y,x]=ind2sub(size(temp2),max_idx);
    c2(n) = c2(n)-pixel_dist + x - 1+1;
    r2(n) = r2(n) - pixel_dist + y - 1+1;

```

```

n = 3;
%bottom left
temp3 = croptemp((r2(n)-pixel_dist):(r2(n)+pixel_dist),(c2(n)-pixel_dist):(c2(n)+pixel_dist),1);
[max_num,max_idx] = max(temp3(:));
[y,x]=ind2sub(size(temp3),max_idx)
c2(n) = c2(n)-pixel_dist + x - 1-1;
r2(n) = r2(n) - pixel_dist + y - 1+1;

n = 4;
%top left
temp = croptemp((r2(n)-pixel_dist):(r2(n)+pixel_dist),(c2(n)-pixel_dist):(c2(n)+pixel_dist),1);
[max_num,max_idx] = max(temp(:));
[y,x]=ind2sub(size(temp),max_idx);
c2(n) = c2(n)-pixel_dist + x - 1-1;
r2(n) = r2(n) - pixel_dist + y - 1-1;

%%
%% Cropping and Centering New Transformed Image

scatter(c2,r2,'MarkerEdgeColor',[1 0 0])

%tform = maketform('projective',[c2/1024*320 r2/1024*240],[c1 r1]); %calculates transform coefficients to map
FROM c2/r2 (thermal camera ref frame) TO c1/r1 (projector reference frame)

tform = maketform('projective',[c2 r2],[c1 r1]); %calculates transform coefficients to map FROM c2/r2 (thermal
camera ref frame) TO c1/r1 (projector reference frame)

% should c1/r1 be c1 = [1;1024;1024;1]; 4 corners x-value ?
%      r1 = [768;768;1;1]; 4 corners y-value
%
disp(tform)

% Get Transformation Matrix

```

```

T = tform.tdata.T;

disp(T)

transform = projective2d(T);

fig4 = figure(6)

[CHtran, xflref] = imwarp(croptemp(:,:,1),transform); %2D projective transform from thermal camera to projector
reference frame?

image(CHtran,'CDataMapping','scaled') % displays transformed image cdatamapping 'scaled' just controls how the
colors display

[c3,r3,P3] = impixel();

%% this means we are only selecting the small rectangle currently being

%% sintered, - not the entire image

%% select projector area

    n = 1;

    %bottom left

    temp1 = CHtran((r3(n)-pixel_dist):(r3(n)+pixel_dist),(c3(n)-pixel_dist):(c3(n)+pixel_dist),1);

    [max_num,max_idx] = max(temp1(:));

    [y,x]=ind2sub(size(temp1),max_idx);

    c3(n) = c3(n)-pixel_dist + x - 1-1;

    r3(n) = r3(n) - pixel_dist + y - 1+1;

    n = 2;

    %bottom right

    temp2 = CHtran((r3(n)-pixel_dist):(r3(n)+pixel_dist),(c3(n)-pixel_dist):(c3(n)+pixel_dist),1);

    [max_num,max_idx] = max(temp2(:));

    [y,x]=ind2sub(size(temp2),max_idx);

    c3(n) = c3(n)-pixel_dist + x - 1+1;

    r3(n) = r3(n) - pixel_dist + y - 1+1;

    n = 3;

    %top right

    temp3 = CHtran((r3(n)-pixel_dist):(r3(n)+pixel_dist),(c3(n)-pixel_dist):(c3(n)+pixel_dist),1);

    [max_num,max_idx] = max(temp3(:));

    [y,x]=ind2sub(size(temp3),max_idx)

```

```

c3(n) = c3(n)-pixel_dist + x - 1+1;
r3(n) = r3(n) - pixel_dist + y - 1-1;

n = 4;
%top left
temp = CHtran((r3(n)-pixel_dist):(r3(n)+pixel_dist),(c3(n)-pixel_dist):(c3(n)+pixel_dist),1);
[max_num,max_idx] = max(temp(:));
[y,x]=ind2sub(size(temp),max_idx);
c3(n) = c3(n)-pixel_dist + x - 1-1;
r3(n) = r3(n) - pixel_dist + y - 1-1;

hold on
scatter(c3,r3,'MarkerEdgeColor',[1 0 0])
pause(10)
% close(fig4)
% close(fig5)

%% writing calibration file
% Replacing T matrix
replaceLineStart = 4;
myformat = '%12.4f %12.4f %12.4f\r\n';
row1 = T(1,:);
row2 = T(2,:);
row3 = T(3,:);

fileID = fopen('config.txt','r+');
for k=1:(replaceLineStart-1);
    fgetl(fileID)
end

fseek(fileID,0,'cof');
fprintf(fileID, myformat, row1);

```

```
fseek(fileID,0,'cof');  
fprintf(fileID, myformat, row2);  
fseek(fileID,0,'cof');  
fprintf(fileID, myformat, row3);  
  
for k=1:7;  
    fgetl(fileID)  
end  
  
myformat2 = '%5.0f %5.0f %5.0f %5.0f\r\n';  
fseek(fileID,0,'cof');  
fprintf(fileID, myformat2, c3);  
fgetl(fileID)  
  
fseek(fileID,0,'cof');  
fprintf(fileID, myformat2, r3);  
fclose(fileID);  
  
type config.txt
```